Resonance Hyper-Raman Characterization of Nonlinear Chromophores

A Dissertation Presented for the

Doctor of Philosophy

Degree

The University of Tennessee, Knoxville

Christopher Bennett Milojevich

May 2013

DEDICATION

I dedicate this work to my son, Isaac Dmitry Milojevich. With the hopes that this will keep you from knowing the pain of working with a Ti: Sapphire laser.

ACKNOWLEDGEMENTS

Thank you to my advisor, Dr. Jon P. Camden, for his guidance and patience with an upstart graduate student; it was a pretty good five years. A very special thanks goes to Allyn Milojevich, the most understanding and guiding wife a man could ever want, who has been most instrumental in keeping my sanity together the last few years. This would not have been possible without her. And finally, I wish to extend my thanks to my committee, Dr. Michael Sepaniak, Dr. Jeffrey Kovac, and Dr. Zhili Zhang for their support and guidance.

ABSTRACT

Hyper-Raman spectroscopy is a nonlinear optical probe which can be used to explore the multi-photon properties of molecules. Three studies are presented in this dissertation. The first study is a combined experimental investigation of the surface-enhanced hyper-Raman scattering with a theoretical study of the electronic states of the Rhodamine 6G molecule. This study demonstrates that hyper-Raman spectroscopy can be used to probe electronic states which are one-photon inaccessible. The second study involves a comparison of experimentally measured resonance hyper-Raman spectra to first-principles calculations of the resonance hyper-Raman scattering. This study shows the utility of coupling hyper-Raman spectroscopy and hyper-Raman calculations to define the multi-photon properties of the molecule. The final study compares the experimentally collected surface-enhanced hyper-Raman spectra of Rhodamine 6G to the theoretical simulations of the resonance hyper-Raman for identical excitation energies. In this study, the mechanism of vibronic coupling in the hyper-Raman effect is fully explained, demonstrating the capability of hyper-Raman spectroscopy predicting the two-photon absorption mechanism.

TABLE OF CONTENTS

INTRODUCTION 1

Statement of purpose 1

Literature Background 2

Hyper-Raman Effect and Surface Enhancements 2

Surface-enhanced Hyper-Raman Scattering (SEHRS) 4

Resonance Hyper-Raman (RHR) 5

Rhodamine dyes 6

Surface Enhanced Resonance Hyper-Raman of Rhodamine 6G 7

Chapter Summaries 11

INTRODUCTION REFERENCES 13

CHAPTER I 24

Abstract 25

Published Work 26

Experimental Section 34

References for Chapter I 35

Appendix for Chapter I 37

I. Fitting of the Experimental SEHRS Spectra 37

II. Concentration study 37

III. Theoretical Methods 37

IV. Comparison of Theory and Experiment 43

V. References for Appendix 45

CHAPTER II 46

Abstract 47

Published Work 48

REFERENCES 57

Chapter II Appendix 60

I. Experimental Methods 60

Experimental Set-up 60

Nanoparticle cluster synthesis 61

RHR measurements 61

SEHRS measurements 61

II. Theoretical Methods 62

References for Appendix 65

CHAPTER III 66

Abstract 67

Introduction 68

Nonlinear Spectroscopy of Rhodamine 6G 70

Resonance Hyper-Raman Calculations 74

Experimental Methods 78

Experimental Set-up 78

SERS/SEHRS sample preparation and use 78

Theoretical Methods 80

Results 83

Vibronic Coupling in Resonance Hyper-Raman Spectra 83

One- and Two-photon Absorption Spectra: Theory and Experiment Comparison 88

Origin of the non-Condon Scattering 91

Conclusion 95

CHAPTER III REFERENCES 96

CONCLUSION 105

VITA 106

LIST OF FIGURES

Figure 1. A Jablonski diagram for both Raman and hyper-Raman spectroscopies indicates the molecular transitions in each. Excitation by an single incident photon ($2\omega_0$) in Raman or two incident photons ($\omega_0 + \omega_0$) in hyper-Raman leads to excitation of the molecule to a virtual state. Subsequently, the molecule relaxes to the ground state, while scattering a photon ($2\omega_0 - \omega_{vib}$). 3

Figure 2. A comparison of SERS (top, P = 300 μW, t_{acq} = 5 s) and SEHRS (bottom, P = 6 mW, t_{acq} = 120 s) of R6G (10^{-6} M) on aggregated Ag colloids taken at excitations of 514 and 1028 nm, respectively. 8

Figure 3. The one-photon absorbance and two-photon excitation spectra[60] are shown for Rhodamine 6G. Also indicated are two transitions within the molecule: S_1, which is one and two-photon accessible, and S_2, which is only two-photon accessible. 9

Figure 4. Selected (4 of 20) surface enhanced hyper-Raman spectra (SEHRS) obtained from R6G on silver colloids for wavelengths between 750 and 1050 nm. Spectra are reported without background or baseline correction. 28

Figure 5. Theoretical (top) and experimental (middle) one- and two-photon (Ref. 12) absorption spectra for R6G compared with ratios of the 771, 1316, 1535, and 1611 bands to the 1189 band (bottom) obtained from wavelength scanned SEHRS experiments. 29

Figure 6. Frontier orbitals involved in the electronic transitions responsible for the features in the one- and two-photon absorption spectra in Figure 5. Normal mode coordinates and frequencies for the vibrations that experience strong resonance enhancement: 765 for S_1, 1518 for S_2, 1607 for S_3. Frequencies given here are from our DFT calculations. 32

Figure 7. Comparison of the experimental and fitted spectrum obtained for λ_{ex} = 880 nm. 38

Figure 8. SEHRS of R6G on Ag [R6G]=10^{-10} M at 880 nm. Raw data (left) and baseline corrected data (right). 39

Figure 9. Simulated off-resonance hyper-Raman spectrum (top) and experimental SEHRS spectrum obtained at 1050 nm (bottom). 44

Figure 10. Comparison of experimentally measured and theoretically calculated resonance hyper-Raman spectra of R6G at λ=825nm. (a) Resonance hyper-Raman of 10^{-3} M R6G in water, (b) SEHRS of R6G on aggregated silver colloids, (c) TDDFT calculation of the RHR spectrum including both Condon (A-term) and non-Condon (B-term) scattering, (d) calculations including only A-term scattering. The spectra are measured and calculated on resonance with the two photon $S_2 \leftarrow S_0$ transition. 51

Figure 11. Comparison of experimentally measured and theoretically calculated hyper-Raman spectra of R6G for excitation wavelengths between 750 and 1050 nm. An asterisk (*) indicates the 1535 cm^{-1} peak. 52

Figure 12. Comparison of the experimentally measured[15] and theoretically calculated (this work) two-photon absorption spectra of R6G. The ratio of the 1535 cm^{-1} to 1189 cm^{-1} peaks is reproduced from Ref. 8. 55

Figure 13. Non-Condon effects in R6G. The hyper-Raman scattering resonant with the S_1 state is dominated by B_2-scattering where the non-Condon effects is due to the nuclear dependence of the two-photon transition moment. For the S_2 state the hyper-Raman scattering is dominated by non-Condon effects in the one-photon transition moment, B_1 scattering. Depicted for the two electronic states are the normal mode of the 1535cm^{-1} vibration and the corresponding one- and two-photon transition moments. 56

Figure 14. A comparison of SERS (top, P = 300 μW, t_{acq} = 5 s) and SEHRS (bottom, P = 6 mW, t_{acq} = 120 s) of R6G (10^{-6} M) on aggregated Ag colloids taken at excitations of 514 and 1028 nm, respectively. 71

Figure 15. The one-photon absorbance and two-photon excitation spectra[42] are shown for Rhodamine 6G. Also indicated are two transitions within the molecule: S_1, which is one and two-photon accessible, and S_2, which is only two-photon accessib 73

Figure 16. Terms included in the calculation of resonance hyper-Raman spectra. In a both one- and two- photon allowed transition $S_k \leftarrow S_0$, both the two-photon transition dipole (S^{k0}) and one-photon transition dipole (μ^{0k}) are non-zero. However, in cases where the one-photon transition is forbidden/weakly allowed (μ^{0k} is zero or nearly zero) or where the two-photon transition is forbidden/weakly allowed (when S^{k0} is zero or nearly zero), then vibronic coupling may produce non-zero terms ($d\mu^{0k}/dQ d\mu 0k dQ$ and dS^{k0}/dQ, respectively) that contribute to the resonant hyper-Raman calculation at these wavelengths. 76

Figure 17. Experimental set-up for surface-enhanced and bulk Raman and hyper-Raman experiments. An Nd:YAG pumped Ti:Sapphire output is split using a half-wave plate and Glan-Polarizer (labeled GP on diagram). The vertical polarization is sent to a second harmonic generator (SHG) and the horizontal polarization is converted to vertical before entering the scope (using a periscope – not pictured). 79

Figure 18. Comparison of experimental and calculated resonance hyper-Raman spectra at an excitation energy of 19000 cm^{-1} (1030 nm). The contributions to the simulated spectra from the individual resonance hyper-Raman terms are also presented: A term (FC), B_1 term (HT), and B_2-term (HT). At this energy the RHR scattering is dominated by B_1 activity. 85

Figure 19. Comparison of experimental and calculated resonance hyper-Raman spectra at an excitation energy of of 24000 cm^{-1} (810 nm). The contributions to

the simulated spectra from the individual resonance hyper-Raman terms are also presented: A term (FC), B_1 term (HT), and B_2-term (HT). At this energy the RHR scattering is dominated by B_1 activity. 86

Figure 20. Comparison of one-photon absorption spectra (left) to the two-photon absorption spectra[32] (right) of Rhodamine 6G and the electronic transitions excited in the molecular orbitals (middle). The absorption spectra are broken into three parts: a) the experimental absorption spectrum, b) the theory simulated spectrum without vibronic coupling (Lorentzian broadened with 0.10 eV full-width at half maximum), and c) the theory simulated absorption spectra, calculated with FC vibronic coupling (orange) and with FC and HT vibronic coupling (red) spectra. 89

Figure 21. Molecular orbitals involved in the $S_1 \leftarrow S_0$ transition. The transition from HOMO (upper left) to LUMO (lower) is symmetry forbidden for a two-photon transition, as it involves a transition from an asymmetric orbital to a symmetric orbital. However, vibronic coupling of the 1535 cm^{-1} vibration to the HOMO yields asymmetric changes (upper right - red indicates a negative change, green a positive change) in the HOMO which allows a two-photon transition to the symmetric LUMO. 92

Figure 22. Molecular orbitals involved in the $S_2 \leftarrow S_0$ transition. The transition from LUMO (lower) to HOMO-1 (upper left) is symmetry forbidden for a one-photon transition, as it involves a transition from a symmetric orbital to a symmetric

orbital. However, vibronic coupling to the 1535 cm^{-1} vibration yields asymmetric changes (upper right – red indicates a negative change, green a positive change) in the HOMO-1 which allows a two-photon transition to the symmetric LUMO..... 93

INTRODUCTION

Statement of purpose

In 1965, the first observation of hyper-Raman scattering was made. Though groundbreaking, the observed phenomenon was largely ignored by the scientific community; studies in optical spectroscopy mostly concentrated on the linear phenomenon of Raman scattering, exploring it in great detail. In the last decade, however, nonlinear processes such as two-photon fluorescence, second harmonic generation, and coherent anti-Stokes Raman scattering have brought nonlinear optical processes to the forefront of scientific exploration. In this climate, hyper-Raman spectroscopy should serve as a useful tool for probing the various factors that govern these spectroscopies. Currently, however, hyper-Raman spectroscopy is studied by very few research groups and very few papers are published studying the phenomenon each year. As such, the field remains relatively unexplored and wide-open for new and exciting explorations of the nonlinear interactions between light and molecules. The work in this dissertation began with the purpose of exploring the usefulness of hyper-Raman, by demonstrating its capacity to probe the mysteries that surround multi-photon processes in general. By doing so, the investigator hopes to spark a renewed interest in a subject that has been somewhat ignored for almost fifty years.

Literature Background

Hyper-Raman Effect and Surface Enhancements

The hyper-Raman effect was first reported in 1965 by Terhune, Savage, and Maker.[1] The effect is due to the third order tensor in the induced dipole moment equation:

$$\mu_{ind} = \alpha \boldsymbol{E} + \frac{1}{2}\beta \boldsymbol{E}^2 + \cdots$$

where μ_{ind} is the induced dipole in the molecule due to E, the oscillating energy field incident on the molecule; α is the polarizability of the molecule; and β represents the hyperpolarizability of the molecule. The polarizability of the molecule determines the Raman activity of the molecule, whereas the hyper-polarizability defines the hyper-Raman activity of the molecule. Hyper-Raman scattering occurs at $2\omega_0 \pm \omega_{vib}$, where ω_0 is the incident frequency and ω_{vib} is a molecular vibration frequency. The Jablonski diagram for hyper-Raman is shown in Figure 1, which shows the difference in these two energies. As it is a two-photon process, the selection rules for hyper-Raman have been calculated to be different from those of either Raman or IR (both traditional vibrational spectroscopies), allowing improbable IR and Raman vibrations to be probed via hyper-Raman spectroscopy. In 1970, Long and Stanton explored the quantum mechanics of the hyper-Raman effect, stating that hyper-Raman scattering is often overlooked because the hyperpolarizability is generally six orders of magnitude smaller than the polarizability of a molecule.[2] For the same laser

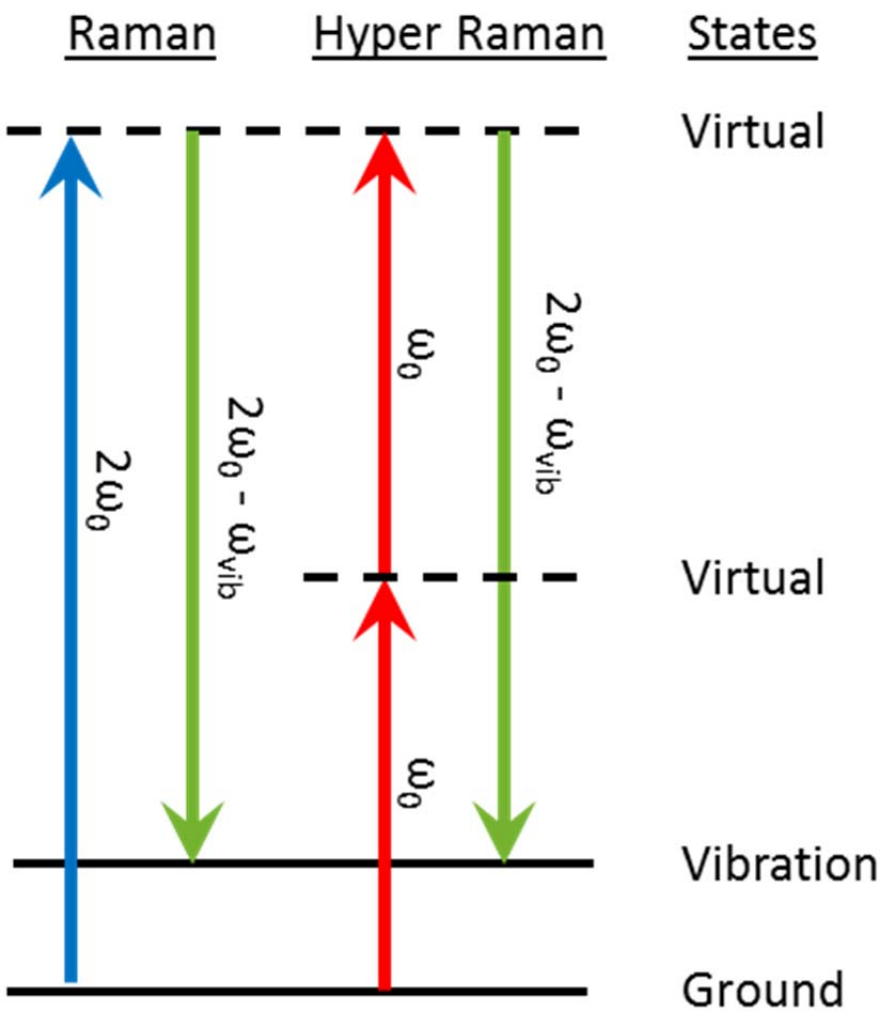


Figure 1. A Jablonski diagram for both Raman and hyper-Raman spectroscopies indicates the molecular transitions in each. Excitation by an single incident photon ($2\omega_0$) in Raman or two incident photons ($\omega_0 + \omega_0$) in hyper-Raman leads to excitation of the molecule to a virtual state. Subsequently, the molecule relaxes to the ground state, while scattering a photon ($2\omega_0 - \omega_{vib}$).

intensity and nonresonant conditions, it has been estimated that hyper-Raman scattering intensities are 5 to 7 orders of magnitude weaker than Raman scattering intensities.[3] For many molecules it is therefore beneficial to make use of enhanced spectroscopy to detect hyper-Raman scattering; either through the use of surface enhancements or resonance conditions.

Surface-enhanced Hyper-Raman Scattering (SEHRS)

The first evidence of coupling hyper-Raman with the electromagnetic enhancement resulting from surface adsorption comes in 1982 from Murphy et al.[4] They employed the electromagnetic enhancement from a silver surface to amplify the weak signal from hyper-Raman by adsorbing sulfur dioxide to silver powder and measuring the hyper-Raman signal generated. The signal measured was weak and decayed rapidly over time to a constant level, which the writers attribute to laser-induced morphology changes of the molecule. Many subsequent experiments reported the surface enhancement of hyper-Raman scattering utilizing many different plasmonic metal surfaces. [5-19] It has been suggested that surface enhancements could lead to the detection of hyper-Raman from a single molecule, but no experiment to date has shown this is possible.[20] However, recent experiments have generated greater amounts of signal from lower laser powers (<0.01 W).[21-22] This is due to recent advances in nanoparticle synthesis, which allow engineering of greater surface enhancements.

Resonance Hyper-Raman (RHR)

In resonance hyper-Raman (RHR) spectroscopy, the incident photon's ($2\omega_0$) energy is chosen to match the excitation energy of the electronic transitions in the molecule. RHR greatly increases the intensity of hyper-Raman scattering, facilitating its measurement in solution.[23] For an order of magnitude comparison, it has been surmised that a resonance hyper-Raman signal may approximate the intensities of a normal Raman signal. [2] RHR studies, however, are still hindered by the small amount of signal generated and the requirement of powerful, pulsed laser systems that also affect studies on non-resonant molecules. [23]

Simulations of RHR scattering are also challenging. The calculations of the resonant first hyperpolarizability for studying RHR scattering are more computationally demanding than the calculations of the resonant polarizability for resonance Raman (RR) scattering. This challenge can be reduced by employing the vibronic theory of RHR scattering developed by Ziegler *et al.*[22] in combination with the time-dependent wavepacket approach.[24-28] The vibronic theory for RHR involves writing the hyperpolarizability of the molecule as a sum of terms: β = A + B + C + …, where A is the Franck-Condon (FC) term, B is the first Herzberg-Teller (HT) term, C is the second HT term, etc. Several studies have demonstrated the utility of the vibronic theory for analyzing experimental observations and the feasibility of RHR simulations for predicting spectra in comparison to available experimental data.[29-34] Furthermore, it has been found that RHR scattering is sensitive to non-Condon effects, possibly more so than

resonance Raman scattering.[30, 34] This feature is related to the selection rules of hyper-Raman scattering, which are complementary to Raman and IR, allowing forbidden IR and Raman-active vibrations to be hyper-Raman active.

Rhodamine dyes

Rhodamine, as a xanthene derivative, is one of the most popular molecules to modify as a two-photon dye.[35-36] As a class of molecules, Rhodamine dye derivatives have had a long and complex history. The first paper on Rhodamine was published in 1905, and discusses synthesis and the use of Rhodamine as a chelating agent for mercury ions.[37] In later decades, the base Rhodamine molecule was modified and functionalized into many different derivations, including Rhodamine 6G (R6G), which has proved effective as a biological stain in cancerous growths,[38] as a fluorescence probe in heavy metal detection,[39] and as a gain medium for dye laser systems.[40] Due to their high photostability, Rhodamine dyes have been extensively utilized in various types of single-molecule[41-43] and fluorescence-tagging spectroscopies.[44-45] Rhodamine dyes or derivatives have recently been used as two-photon fluorescence probes for mercury ions in live cells,[46] as multi-photon probes for exploring diffusion in vivo skin samples,[47] and as benchmark molecules in two-photon excitation systems[48]. A common wavelength of interest in biological studies involving Rhodamine is 800 nm, as many biological tissues are fairly transparent at both the fundamental and second harmonic (~400 nm).[46] In later years, it also became a staple in Raman spectroscopy[49-50] and specifically surface-enhanced Raman scattering

(SERS)[16, 51-54], as R6G was shown to have an extremely large Raman cross-section when excited on resonance (e.g. at 514 or 532 nm)[51]. Its large Raman cross-section[16] made R6G the perfect candidate for the first single-molecule SERS experiment.[42]

Surface Enhanced Resonance Hyper-Raman of Rhodamine 6G

The first SEHRS of R6G, reported in 1982 by Baranov and Bobovich,[55] dates from the earliest days of surface-enhanced vibrational spectroscopy. Their pioneering study compared SEHRS and SERS of R6G at excitation wavelengths of 1064 and 532 nm and found dramatic differences between the two. Figure 2 displays SEHRS spectra at 1028 nm and SERS spectra at 514 nm for R6G, illustrating these differences, even though both spectra are measured at equivalent frequencies for the respective processes. Even 30 years after their discovery, the origin of these differences has not been satisfactorily explained, despite numerous studies of the two-photon properties of R6G. [8, 19, 55-59] To further emphasize the differences in these spectra, a short discussion follows about differences observed in the one- and two-photon absorption spectra.

In Figure 3 the one- and two-photon[60] absorption (TPA) spectra of R6G between 18000 and 27000 wavenumbers are presented. We further review explanations previously invoked to explain the difference between the SERS and SEHRS spectra. It is well known that the SERS spectrum of Rhodamine 6G at 18900 cm^{-1} (532 nm) is resonant; this can be confirmed by the strong absorption band

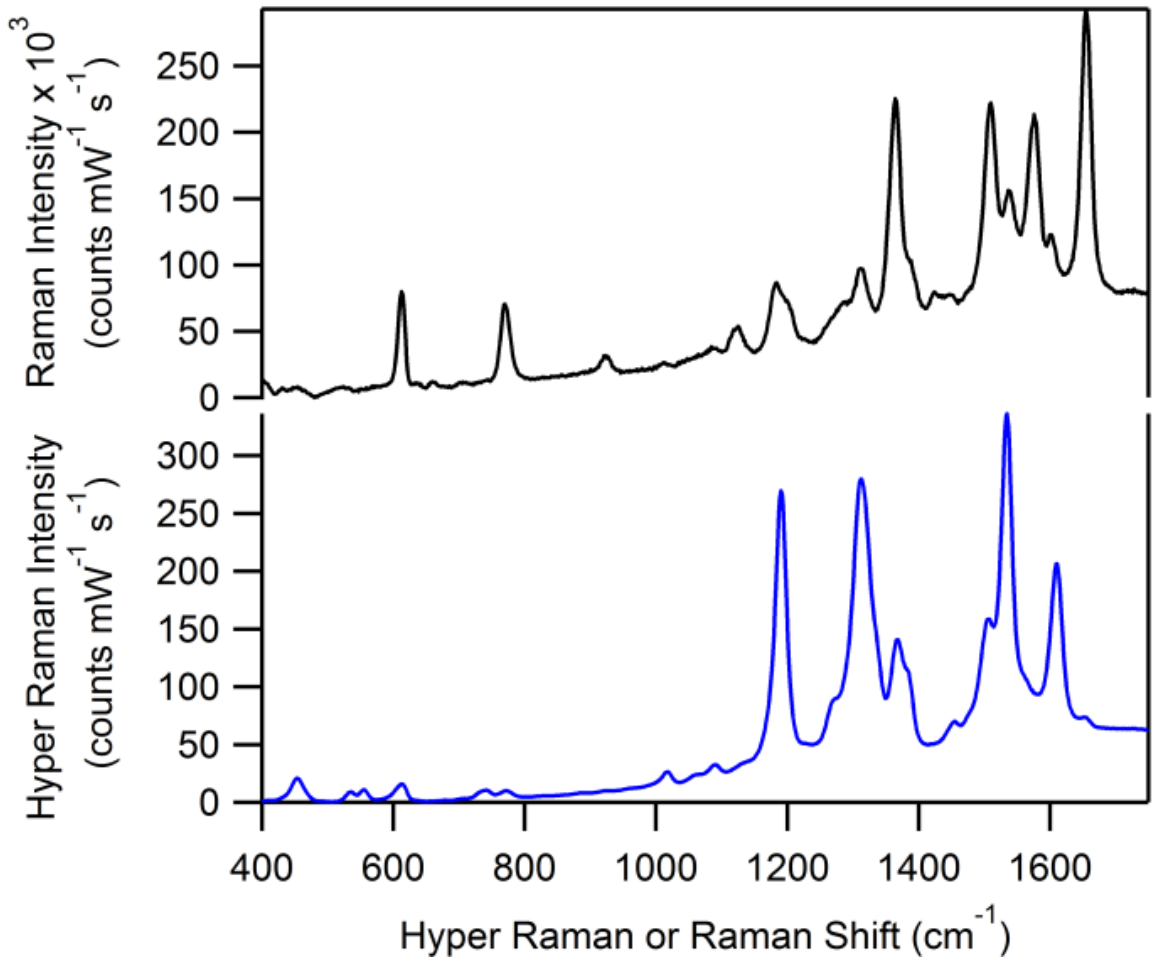


Figure 2. A comparison of SERS (top, P = 300 μW, t_{acq} = 5 s) and SEHRS (bottom, P = 6 mW, t_{acq} = 120 s) of R6G (10^{-6} M) on aggregated Ag colloids taken at excitations of 514 and 1028 nm, respectively.

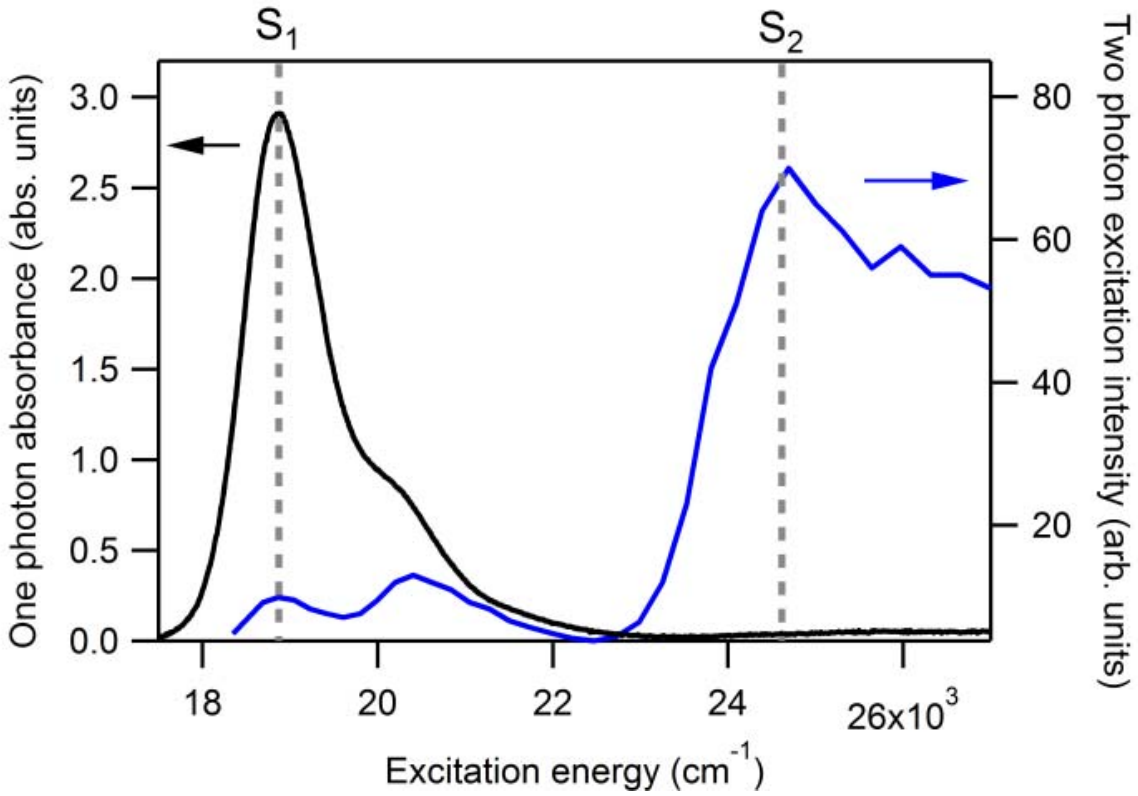


Figure 3. The one-photon absorbance and two-photon excitation spectra[60] are shown for Rhodamine 6G. Also indicated are two transitions within the molecule: S_1, which is one and two-photon accessible, and S_2, which is only two-photon accessible.

shown in the one-photon absorption (OPA) spectrum. This absorption in R6G is attributed to S_1, the first excited singlet state.

When the first observation of the SEHRS of R6G was made at 18900 cm^{-1} (1064 nm), it was also assumed to be resonant, due mainly to the strength of the signal generated.[55] This assumption was later confirmed, however, by the observation of a peak in the TPA spectrum centered around 18900 cm^{-1}. These observations suggested that the S_1 transition is both one- and two-photon allowed and therefore the $S_1 \leftarrow S_0$ electronic transition was not governed by the parity of the states involved. This seeming lack of symmetry elements for S_1 and S_0; however, implied that the resonance enhanced SERS and SEHRS spectra should be identical, a fact which is contrary to experimental evidence. As seen in Figure 2, the two spectra are very different: they share very few common peaks and the peak intensities are drastically different. There have been multiple attempts to explain how the two spectra can be resonant, and yet completely different. First, it was assumed that the silver surface "extends" the one photon absorption to energies below 10000 cm^{-1}.[61] This theory, however, can be rejected as the TPA spectrum has an absorption in this region, despite the fact that there is no silver in the sample. Next, it was suggested that the surface provides greater enhancements for the hyper-Raman spectrum and those enhancements selectively enhanced different modes.[62] The latter theory can be rejected, as we have shown that the SEHRS spectrum is identical to the non-surface enhanced

spectrum, at least for wavelengths where the two can be measured.[63] Later, it was proposed that the surface distorts the molecule, to create non-symmetry for a mode that normally has symmetry. In the two-photon spectrum, it was assumed that the anion present distorted the molecule to present the same non-symmetry.[35] In the absorption spectra (Figure 3), a two-photon absorption can be observed at 25000 wavenumbers, which is not observed in the one-photon spectrum. It seems unlikely that a change in symmetry would be created in the molecule that permits only the two-photon transition to be allowed. Furthermore, calculations of the molecule in free space show the same absorptions, indicating that the solvent effects are negligible in providing these absorptions. The question as to how the Rhodamine molecule can be resonant in both Raman at 532 nm and hyper-Raman at 1064 nm remained unsolved, until the publications in this dissertation.

Chapter Summaries

The chapters in this dissertation outline a study conducted on one nonlinear dye molecule, Rhodamine 6G. The study begins in Chapter I with a paper published that identifies the use of resonance hyper-Raman to map the second excited state of Rhodamine 6G. Chapter II outlines the discovery, through coupling of hyper-Raman simulations and experiments, that vibrations of the Rhodamine molecule enhance the two-photon fluorescence of the molecule. This discovery is unique, in that most molecules do not exhibit these enhancements at a

measurable strength. In Chapter III, the enhancement is elucidated through the use of molecular orbital calculations. Further, the mechanism which allows such enhancements is brought to light. Finally, in Chapter IV, hyper-Raman spectroscopy experiments and simulations are compared to experiments and simulations of IR and Raman spectroscopies. In a complicated molecule such as Rhodamine, it is difficult to discern the properties of each, but the discussion does illuminate how a complex molecule can appear to have modes which defy the known selection rules for each spectroscopy.

INTRODUCTION REFERENCES

1. Terhune, R. W.; Maker, P. D.; Savage, C. M., Measurements of nonlinear light scattering. *Physical Review Letters* **1965,** *14* (17), 681-&.

2. Long, D. A.; Stanton, L., Studies of non-linear phenomena; i. Theory of the hyper raman effect. *Procedings of the Royal Society of London A* **1970,** *318*, 441-457.

3. Ziegler, L. D., Hyper-raman spectroscopy. *Journal of Raman Spectroscopy* **1990,** *21* (12), 769-779.

4. Murphy, D. G.; Von Raben, K. U.; Chang, R. K., Surface-enhanced hyper-raman scattering from sulfate adsorbed on ag powder. *Chemical Physics Letters* **1982,** *85* (1), 43-47.

5. Golab, J. T.; Sprague, J. R.; Carron, K. T.; Schatz, G. C.; Van Duyne, R. P., A surface enhanced hyper-raman scattering study of pyridine adsorbed onto silver: Experiment and theory. *Journal of Chemical Physics* **1988,** *88* (12), 7942-7951.

6. Itoh, T.; Yoshikawa, H.; Yoshida, K.; Biju, V.; Ishikawa, M., Evaluation of electromagnetic enhancement of surface enhanced hyper raman scattering using plasmonic properties of binary active sites in single ag nanoaggregates. *Journal of Chemical Physics* **2009,** *130*, 214706.

7. Carron, K. T. Surface enhanced resonance raman, resonance hyper-raman, and hyper-raman spectroscopy of molecules adsorbed to thin metal films. Northwestern University, 1985.

8. Baranov, A. V.; Bobovich, Y. S., Super-enhanced hyper-raman scattering from dyes adsorbed on colloidal silver particles. *Jetp Lett.* **1982,** *36* (8), 339-343.

9. Hulteen, J. C.; Young, M. A.; Van Duyne, R. P., Surface-enhanced hyper-raman scattering (sehrs) on ag film over nanosphere (fon) electrodes: Surface symmetry of centrosymmetric adsorbates. *Langmuir* **2006,** *22* (25), 10354-10364.

10. Ikeda, K.; Takase, M.; Sawai, Y.; Nabika, H.; Murakoshi, K.; Uosaki, K., Hyper-raman scattering enhanced by anisotropic dimer plasmons on artificial nanostructures. *Journal of Chemical Physics* **2007,** *127* (11).

11. Itoh, T.; Ozaki, Y.; Yoshikawa, H.; Ihama, T.; Masuhara, H., Hyper-rayleigh scattering and hyper-raman scattering of dye-adsorbed silver nanoparticles induced by a focused continuous-wave near-infrared laser. *Applied Physics Letters* **2006,** *88* (8).

12. Kneipp, J.; Kneipp, H.; Wittig, B.; Kneipp, K., One- and two-photon excited optical ph probing for cells using surface-enhanced raman and hyper-raman nanosensors. *Nano Letters* **2007,** *7* (9), 2819-2823.

13. Kneipp, K.; Kneipp, H.; Seifert, F., Near-infrared excitation profile study of surface-enhanced hyper-raman scattering and surface-enhanced raman-scattering by means of tunable mode-locked ti-sapphire laser excitation. *Chem. Phys. Lett.* **1995,** *233* (5-6), 519-524.

14. Leng, W. N.; Woo, H. Y.; Vak, D.; Bazan, G. C.; Kelley, A. M., Surface-enhanced resonance raman and hyper-raman spectroscopy of water-soluble substituted stilbene and distyrylbenzene chromophores. *Journal of Raman Spectroscopy* **2006,** *37* (1-3), 132-141.

15. Leng, W. N.; Yasseri, A. A.; Sharma, S.; Li, Z. Y.; Woo, H. Y.; Vak, D.; Bazan, G. C.; Kelley, A. M., Silver nanocrystal-modified silicon nanowires as substrates for surface-enhanced raman and hyper-raman scattering. *Analytical Chemistry* **2006,** *78* (17), 6279-6282.

16. Li, W. H.; Li, X. Y.; Yu, N. T., Surface-enhanced resonance hyper-raman scattering and surface-enhanced resonance raman scattering of dyes adsorbed on silver electrode and silver colloid: A comparison study. *Chem. Phys. Lett.* **1999,** *312* (1), 28-36.

17. Lipscomb, L. A.; Nie, S.; Feng, S.; Yu, N. T., Surface-enhanced hyper-raman spectroscopy with a picosecond laser - gold and copper colloids. *Chem. Phys. Lett.* **1990,** *170* (5-6), 457-461.

18. Yang, W.; Hulteen, J.; Schatz, G. C.; Van Duyne, R. P., A surface-enhanced hyper-raman and surface-enhanced raman scattering study of trans-1,2-bis(4-pyridyl)ethylene adsorbed onto silver film over nanosphere electrodes. Vibrational assignments: Experiment and theory. *Journal of Chemical Physics* **1996,** *104* (11), 4313-4323.

19. Yu, N. T.; Nie, S. M.; Lipscomb, L. A., Surface-enhanced hyper-raman spectroscopy with a picosecond laser - new vibrational information for noncentrosymmetric carbocyanine molecules adsorbed on colloidal silver. *Journal of Raman Spectroscopy* **1990,** *21* (12), 797-802.

20. Kneipp, K.; Kneipp, H.; Itzkan, I.; Dasari, R. R.; Feld, M. S., Surface-enhanced non-linear raman scattering at the single-molecule level. *Chemical Physics* **1999,** *247* (1), 155-162.

21. Itoh, T.; Yoshikawa, H.; Yoshida, K.; Biju, V.; Ishikawa, M., Spectral variations in background light emission of surface-enhanced resonance hyper raman scattering coupled with plasma resonance of individual silver nanoaggregates (vol 133, 124704, 2010). *Journal of Chemical Physics* **2010,** *133* (14).

22. Leng, W. N.; Kelley, A. M., Surface-enhanced hyper-raman spectra and enhancement factors for three sers chromophores. Sehrs spectra on ag films at

pulse energies below 2 pj. *Journal of the American Chemical Society* **2006,** *128* (11), 3492-3493.

23. Kelley, A. M., Resonance raman and resonance hyper-raman intensities: Structure and dynamics of molecular excited states in solution. *Journal of Physical Chemistry A* **2008,** *112* (47), 11975-11991.

24. Chu, L. Q.; Masyuko, R.; Sweedler, J. V.; Bohn, P. W., Base-induced delignification of miscanthus x giganteus studied by three-dimensional confocal raman imaging. *Bioresour. Technol.* **2010,** *101* (13), 4919-4925.

25. Eronen, P.; Osterberg, M.; Jaaskelainen, A. S., Effect of alkaline treatment on cellulose supramolecular structure studied with combined confocal raman spectroscopy and atomic force microscopy. *Cellulose* **2009,** *16* (2), 167-178.

26. Yamauchi, S.; Sakai, Y.; Watanabe, Y.; Kubo, M. K.; Matsue, H., Distribution of boron in wood treated with aqueous and methanolic boric acid solutions. *J. Wood Sci.* **2007,** *53* (4), 324-331.

27. Edwards, H. G. M.; Sibley, M. G.; Derham, B.; Heron, C. P., Raman spectroscopy of archaeological samples from the barber-surgeon's medicine chest on the mary rose. *Journal of Raman Spectroscopy* **2004,** *35* (8-9), 746-753.

28. Shen, Q.; Rahiala, H.; Rosenholm, J. B., Evaluation of the structure and acid-base properties of bulk wood by ft-raman spectroscopy. *J. Colloid Interface Sci.* **1998,** *206* (2), 558-568.

29. Kelley, A. M.; Leng, W. N.; Blanchard-Desce, M., Resonance hyper-raman scattering from conjugated organic donor-acceptor "push-pull" chromophores with large first hyperpolarizabilities. *Journal of the American Chemical Society* **2003,** *125* (35), 10520-10521.

30. Tu, Q.; Chang, C., Diagnostic applications of raman spectroscopy. *Nanomed.-Nanotechnol. Biol. Med.* **2012,** *8* (5), 545-558.

31. Casadio, F.; Leona, M.; Lombardi, J. R.; Van Duyne, R., Identification of organic colorants in fibers, paints, and glazes by surface enhanced raman spectroscopy. *Accounts Chem. Res.* **2010,** *43* (6), 782-791.

32. Leng, W.; Kelley, A. M., Hyper-rayleigh and hyper-raman scatterings with intermediate and two-photon resonances. *Journal of Chemical Physics* **2007,** *127* (16).

33. Leng, W.; Kelley, A. M., Resonance hyper-raman spectra of zinc phthalocyanine. *Journal of Physical Chemistry A* **2008,** *112* (26), 5925-5929.

34. Milojevich, C. B.; Silverstein, D. W.; Jensen, L.; Camden, J. P., Probing two-photon properties of molecules: Large non-condon effects dominate the

resonance hyper-raman scattering of rhodamine 6g. *Journal of the American Chemical Society* **2011,** *133* (37), 14590-2.

35. Wakebe, T.; Van Keuren, E., The excitation spectra of two-photon induced fluorescence in xanthene dyes. *Jpn. J. Appl. Phys. Part 1 - Regul. Pap. Short Notes Rev. Pap.* **1999,** *38* (6A), 3556-3561.

36. Wolff, J. J.; Wortmann, R., Organic materials for second-order non-linear optics. In *Advances in physical organic chemistry*, Bethell, D., Ed. Academic Press: 1999; Vol. Volume 32, pp 121-217.

37. Noelting, E.; Dziewonski, K., Information on rhodamines first announcement. *Ber. Deutsch. Chem. Ges.* **1905,** *38*, 3516-3527.

38. Lewis, M. R.; Goland, P. P.; Sloviter, H. A., Selective action of certain dyestuffs on sarcomata and carcinomata. *Anat. Rec.* **1946,** *96* (2), 201-220.

39. Sagi, S. R.; Rao, G. G., Ferrimetric determination of molybdenum(v) using rhodamine 6g as fluorescent indicator. *Fres. Zeit. Fur Anal. Chem.* **1962,** *188* (3), 164-168.

40. Shank, C. V.; Dienes, A.; Silfvast, W. T., Single pass gain of exciplex 4-mu and rhodamine 6g dye laser amplifiers. *Appl. Phys. Lett.* **1970,** *17* (7), 307-310.

41. Ganne-Chedeville, C.; Jaaskelainen, A. S.; Froidevaux, J.; Hughes, M.; Navi, P., Natural and artificial ageing of spruce wood as observed by ftir-atr and uvrr spectroscopy. *Holzforschung* **2012,** *66* (2), 163-170.

42. Nie, S. M.; Emory, S. R., Probing single molecules and single nanoparticles by surface-enhanced raman scattering. *Science* **1997,** *275* (5303), 1102-1106.

43. Dieringer, J. A.; Lettan, R. B.; Scheidt, K. A.; Van Duyne, R. P., A frequency domain existence proof of single-molecule surface-enhanced raman spectroscopy. *Journal of the American Chemical Society* **2007,** *129* (51), 16249-16256.

44. Fontaine, M.; Elmquist, W. F.; Miller, D. W., Use of rhodamine 123 to examine the functional activity of p-glycoprotein in primary cultured brain microvessel endothelial cell monolayers. *Life Sci.* **1996,** *59* (18), 1521-1531.

45. Liu, W. Y.; Li, H. Y.; Lv, H. S.; Zhao, B. X.; Miao, J. Y., A rhodamine chromene-based turn-on fluorescence probe for selectively imaging cu2+ in living cell. *Spectroc. Acta Pt. A-Molec. Biomolec. Spectr.* **2012,** *95*, 658-663.

46. Lee, J. H.; Lim, C. S.; Tian, Y. S.; Han, J. H.; Cho, B. R., A two-photon fluorescent probe for thiols in live cells and tissues. *Journal of the American Chemical Society* **2010,** *132* (4), 1216-+.

47. Masanta, G.; Lim, C. S.; Kim, H. J.; Han, J. H.; Kim, H. M.; Cho, B. R., A mitochondrial-targeted two-photon probe for zinc ion. *Journal of the American Chemical Society* **2011,** *133* (15), 5698-5700.

48. So, P. T. C.; Dong, C. Y.; Masters, B. R.; Berland, K. M., Two-photon excitation fluorescence microscopy. *Annual Review of Biomedical Engineering* **2000,** *2*, 399-429.

49. Devlin, J. P.; Rockley, M. G., Raman-spectra in electronic excited-state - cars spectra of lasing rhodamine 6g. *Chem. Phys. Lett.* **1978,** *56* (3), 608-610.

50. Majoube, M.; Henry, M., Fourier-transform raman and infrared and surface-enhanced raman-spectra for rhodamine-6g. *Spectroc. Acta Pt. A-Molec. Biomolec. Spectr.* **1991,** *47* (9-10), 1459-1466.

51. Hildebrandt, P.; Stockburger, M., Surface-enhanced resonance raman-spectroscopy of rhodamine-6g adsorbed on colloidal silver. *J. Phys. Chem.* **1984,** *88* (24), 5935-5944.

52. Shim, S.; Stuart, C. M.; Mathies, R. A., Resonance raman cross-sections and vibronic analysis of rhodamine 6g from broadband stimulated raman spectroscopy. *ChemPhysChem* **2008,** *9* (5), 697-699.

53. Michaels, A. M.; Nirmal, M.; Brus, L. E., Surface enhanced raman spectroscopy of individual rhodamine 6g molecules on large ag nanocrystals. *Journal of the American Chemical Society* **1999,** *121* (43), 9932-9939.

54. Zeisel, D.; Deckert, V.; Zenobi, R.; Vo-Dinh, T., Near-field surface-enhanced raman spectroscopy of dye molecules adsorbed on silver island films. *Chem. Phys. Lett.* **1998,** *283* (5-6), 381-385.

55. Cumpston, B. H.; Ananthavel, S. P.; Barlow, S.; Dyer, D. L.; Ehrlich, J. E.; Erskine, L. L.; Heikal, A. A.; Kuebler, S. M.; Lee, I. Y. S.; McCord-Maughon, D.; Qin, J. Q.; Rockel, H.; Rumi, M.; Wu, X. L.; Marder, S. R.; Perry, J. W., Two-photon polymerization initiators for three-dimensional optical data storage and microfabrication. *Nature* **1999,** *398* (6722), 51-54.

56. Larson, D. R.; Zipfel, W. R.; Williams, R. M.; Clark, S. W.; Bruchez, M. P.; Wise, F. W.; Webb, W. W., Water-soluble quantum dots for multiphoton fluorescence imaging in vivo. *Science* **2003,** *300* (5624), 1434-1436.

57. Lee, P. C.; Meisel, D., Adsorption and surface-enhanced raman of dyes on silver and gold sols. *J. Phys. Chem.* **1982,** *86* (17), 3391-3395.

58. Hales, J. M.; Matichak, J.; Barlow, S.; Ohira, S.; Yesudas, K.; Bredas, J. L.; Perry, J. W.; Marder, S. R., Design of polymethine dyes with large third-order optical nonlinearities and loss figures of merit. *Science* **2010,** *327* (5972), 1485-1488.

59. Makarov, N. S.; Drobizhev, M.; Rebane, A., Two-photon absorption standards in the 550-1600 nm excitation wavelength range. *Optics Express* **2008,** *16* (6), 4029-4047.

60. Baranov, A. V.; Bobovich, Y. S.; Petrov, V. I., Surface-enhanced resonance hyper-raman (serhr) spectroscopy of photochromatic molecules. *Journal of Raman Spectroscopy* **1993,** *24*, 695-697.

61. Baranov, A. V.; Bobovich, Y. S., Higher-order surface-enhanced raman-scattering. *Jetp Lett.* **1982,** *35* (4), 181-183.

62. Nie, S. M.; Lipscomb, L. A.; Yu, N. T., Surface-enhanced hyper-raman spectroscopy. *Applied Spectroscopy Reviews* **1991,** *26* (3), 203-276.

63. He, G. S.; Tan, L. S.; Zheng, Q.; Prasad, P. N., Multiphoton absorbing materials: Molecular designs, characterizations, and applications. *Chemical Reviews* **2008,** *108* (4), 1245-1330.

CHAPTER I

PROBING ONE-PHOTON INACCESSABLE ELECTRONIC STATES WITH HIGH SENSITIVITY: WAVELENGTH SCANNED SURFACE ENHANCED HYPER-RAMAN SCATTERING (WS-SEHRS)

A version of this chapter was originally published by Chris B. Milojevich, Daniel W. Silverstein, Lasse Jensen, and Jon P Camden:

Milojevich, C. B., Silverstein, D. W., Jensen, L. and Camden, J. P. (2011), **Probing One-Photon Inaccessible Electronic States with High Sensitivity: Wavelength Scanned Surface Enhanced Hyper-Raman Scattering**. *ChemPhysChem*, 12: 101–103.

The article is represented in the form which it was published, with the exception that the following ChemPhysChem required sections have been removed: Acknowledgements. The supplemental information section of the paper has been added as an appendix. The dissertation author conducted all of the experiments indicated in the paper, designed each of the figures, and specifically authored the Experimental Methods section and experimental portions of the Appendix. The calculations indicated in the paper were conducted by DW Silverstein and L Jensen. All authors contributed equally and approved the final document.

Abstract

A combined experimental and theoretical study of the surface-enhanced hyper-Raman scattering (SEHRS) provides a detailed picture of the electronic excited state of the benchmark Rhodamine 6G molecule. These results demonstrate the

ability of SEHRS to explore excited states that are not easily accessible via one-photon excitation using nonlinear spectroscopy at very low (10^{-10} M) concentrations.

Published Work

Electronic excited states play an essential role in a wide range of molecular processes from biology[1] to molecular electronics.[2] Charge separation, for example, and its subsequent transport, in organic photovoltaics occurs through molecular excited states.[3] Traditionally, experimental characterization of the topology of molecular excited states is achieved through spectroscopic techniques such as resonance Raman scattering.[4] The sensitivity of resonance Raman to details of the excited state potential energy landscape is clearly elucidated in the theory of inelastic light scattering,[5] although ab initio calculations of electronic excited states remain quite challenging.

In some cases, one photon transitions to the electronic state of interest are either very weak or forbidden and thus the methods available for probing these “dark” states are severely restricted. These dark states, however, are often coupled to the bright states and can play a major role in the electronic and nuclear dynamics. Indeed, a recent study of excited state intermolecular proton transfer demonstrated that dark states can directly affect electronic relaxation kinetics, which subsequently alters the product branching ratios.[6] In this communication

we report a method utilizing surface enhanced hyper-Raman scattering (SEHRS) to probe these one-photon inaccessible electronic states for analytes at low concentration (~10^{-10} M). We also demonstrate that a close coupling of time-dependent density functional theory (TDDFT) simulations of the two-photon absorption spectrum and off-resonance hyper-Raman spectra yield important insights into the nature of the probed electronic states.

Hyper-Raman scattering[7] is a type of non-linear light scattering in which a photon at $\omega = 2\omega_0 - \omega_{vib}$ is incoherently scattered, where ω_0 is the laser frequency and ω_{vib} is a vibration characteristic of the material. Hyper-Raman scattering provides information that is complementary to that obtained from IR and Raman; further resonance hyper-Raman provides access to electronic states that are *not* one-photon allowed. While hyper-Raman scattering is an inherently weak process, the signal originating from molecules located near the surface of a plasmonic nanostructure can be enhanced by many orders of magnitude.[8, 9, 10, 11] SEHRS also contains unique information about surface symmetry[12] and can be applied to biological imaging.[13]

SEHRS spectra of Rhodamine 6G (R6G) adsorbed on aggregated silver colloids were recorded for excitation wavelengths between 750-1045 nm in increments of ~15nm. This range spans the two-photon absorption spectrum of R6G[14] and selected (4 of 20) spectra are shown in Figure 4. All spectra are reported *without* baseline or background corrections and typical laser powers were ~5 mW (~63

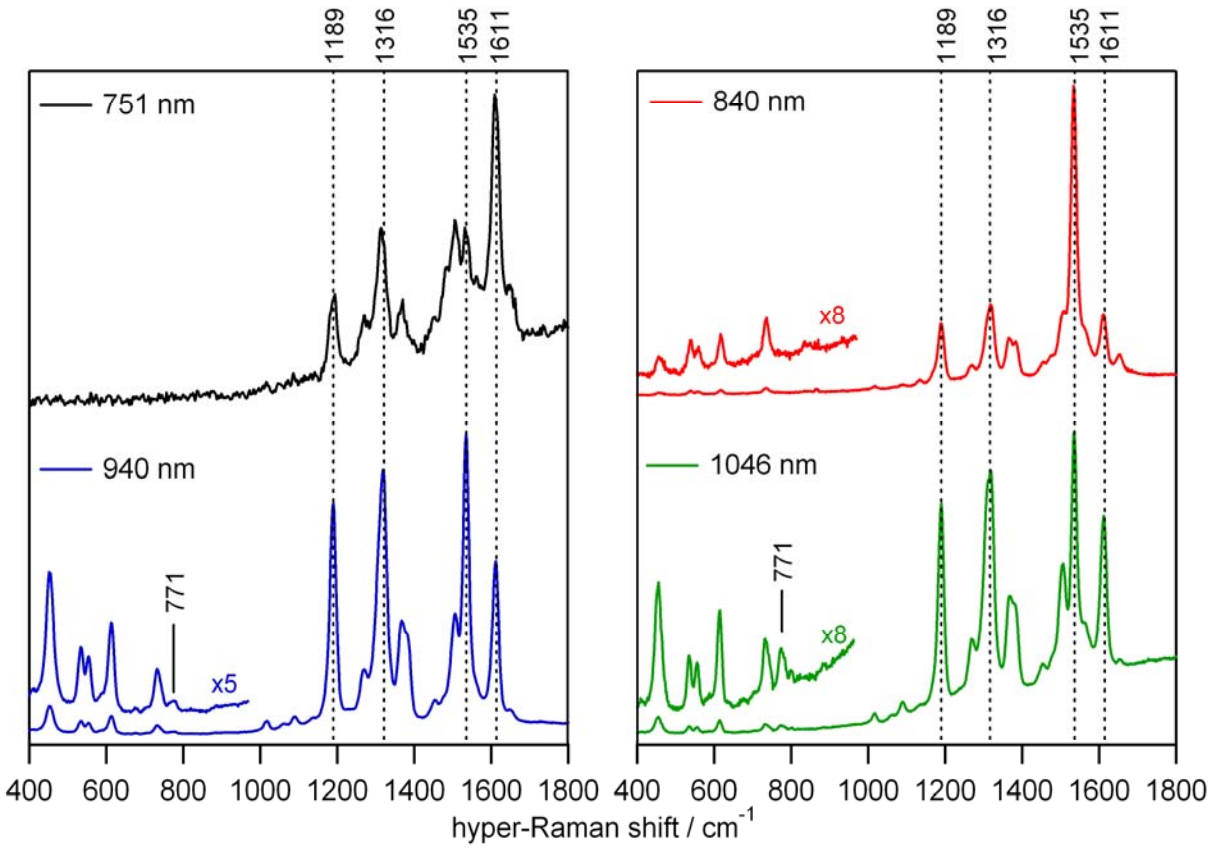


Figure 4. Selected (4 of 20) surface enhanced hyper-Raman spectra (SEHRS) obtained from R6G on silver colloids for wavelengths between 750 and 1050 nm. Spectra are reported without background or baseline correction.

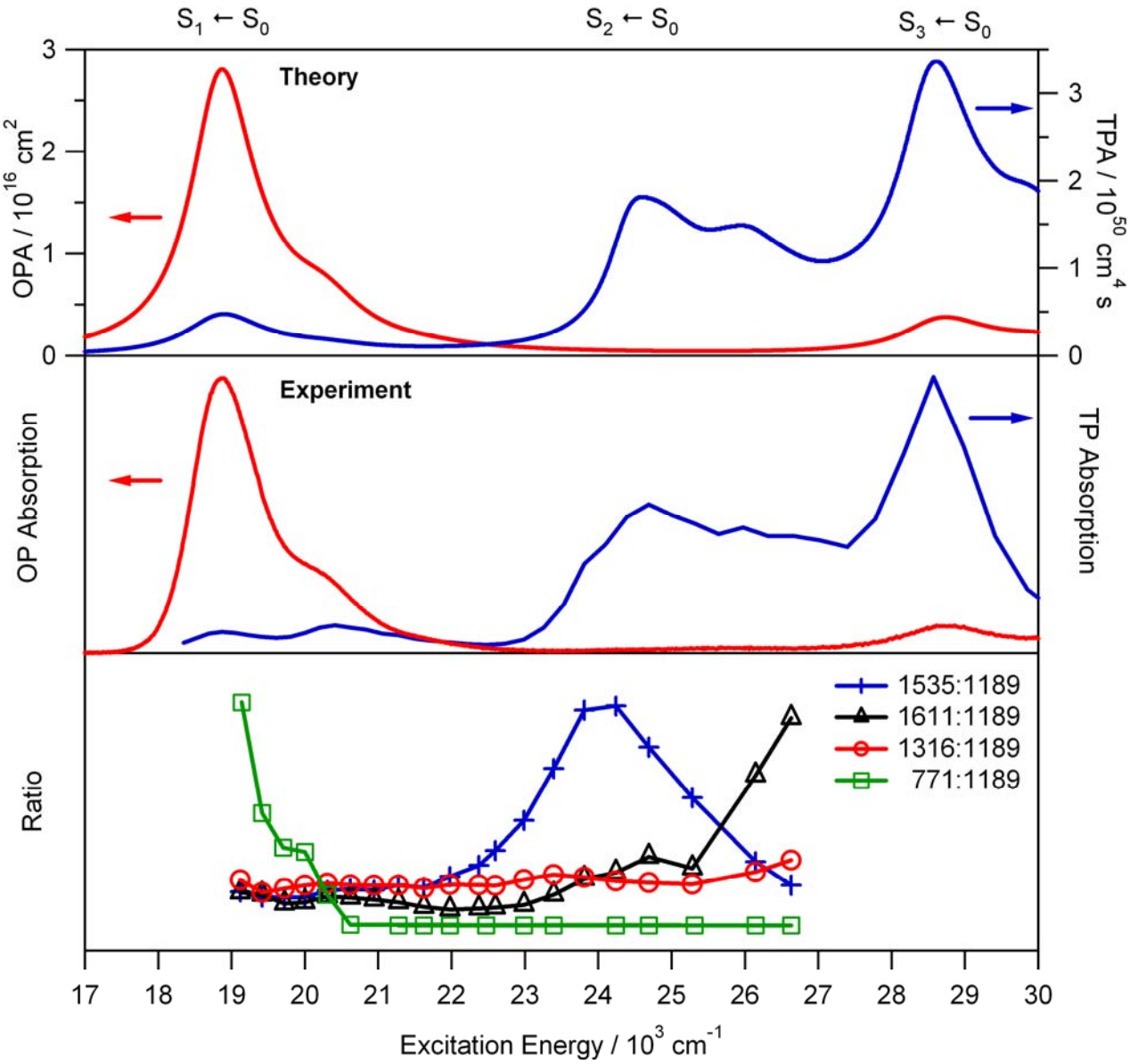


Figure 5. Theoretical (top) and experimental (middle) one- and two-photon (Ref. 12) absorption spectra for R6G compared with ratios of the 771, 1316, 1535, and 1611 bands to the 1189 band (bottom) obtained from wavelength scanned SEHRS experiments.

pJ/pulse) at the sample. The concentration of R6G was 10^{-7} M for the wavelength scanned experiments but we have obtained spectra with [R6G] =10^{-10} M.

In order to systematically explore the changes in the SEHRS spectra as a function of excitation energy, we fit each spectrum to determine peak positions and areas (see SI). The fitted areas were then used to plot ratios of the 771, 1316, 1535, and 1611 bands to the 1189 band as a function of excitation wavelength. Figure 5 compares the experimental and theoretical, one- and two-photon absorption spectrum of R6G with our peak area ratios as a function of excitation energy. The 1189 band was chosen as a reference because it remains mostly constant over the measured range and because the large signal difference between SEHRS and normal hyper-Raman scattering makes calibration to an internal standard difficult.

The ratio 1316:1189 remains constant over the measured range, while the other ratios 771:1189, 1535:1189 and 1611:1189 correlate well with peaks in the two-photon absorption spectrum suggesting these bands experience a resonance enhancement. Further, 1535 peaks in a region where the one-photon absorption cross section is negligible. Our theoretically calculated absorption spectra (Figure 5) are in good agreement with experiment and yield insight into the nature of the responsible excited states. For excitation energies probed here, three excited states, S_1, S_2, and S_3, contribute to the absorption spectra; however, excitation to S_2 is *not* observed in the one-photon spectra. Figure 6 displays the frontier orbitals involved in the electronic transitions $S_1 \leftarrow S_0$, $S_2 \leftarrow S_0$, and $S_3 \leftarrow S_0$. All three states are localized on the xanthene ring region of the R6G molecule and

indeed the major modes observed are vibrations whose motion is concentrated in this area.

To understand in more detail the observed SEHRS spectra we calculated the off-resonance hyper-Raman spectra by numerical differentiation of the static hyperpolarizability obtained from TDDFT. Calculations at this level of theory yield excellent agreement with experimental measurements of the absolute hyper-Raman cross section of water (σ_{TDDFT}=6x10^{-64} cm^4 s photon^{-1} and σ_{expt}=6x10^{-63} cm^4 s photon^{-1} at 840 nm[15]). A comparison of the simulated off-resonance spectrum with the experimental SEHRS spectrum obtained at 1050 nm (shown in SI) yields good agreement with respect to both band positions and intensities. The observed differences are likely due to the neglect of surface orientation[16] and resonance effects in the simulations.

Resonance hyper-Raman scattering can be characterized in terms of Franck-Condon scattering (A-term) and Herzberg-Teller scattering (B-term).[17] If we assume only A-term scattering, the absolute resonance hyper-Raman cross sections for the strongest band of R6G is 1x10^{-59} cm^4 s photon^{-1} on resonance with S_1, 3x10^{-61} cm^4 s/photon on resonance with S_2, and 7x10^{-59} cm^4 s photon^{-1} on resonance with S_3. Thus, the resonance enhancement for R6G arising from the A-term is comparable in magnitude to the strong off-resonance hyper-Raman cross section (6x10^{-60} cm^4 s photon^{-1}) This feature of the scattering occurs because none of the excited states have simultaneously strong one- and two-photon absorption, as observed in the absorption spectra. Calculations of B-term

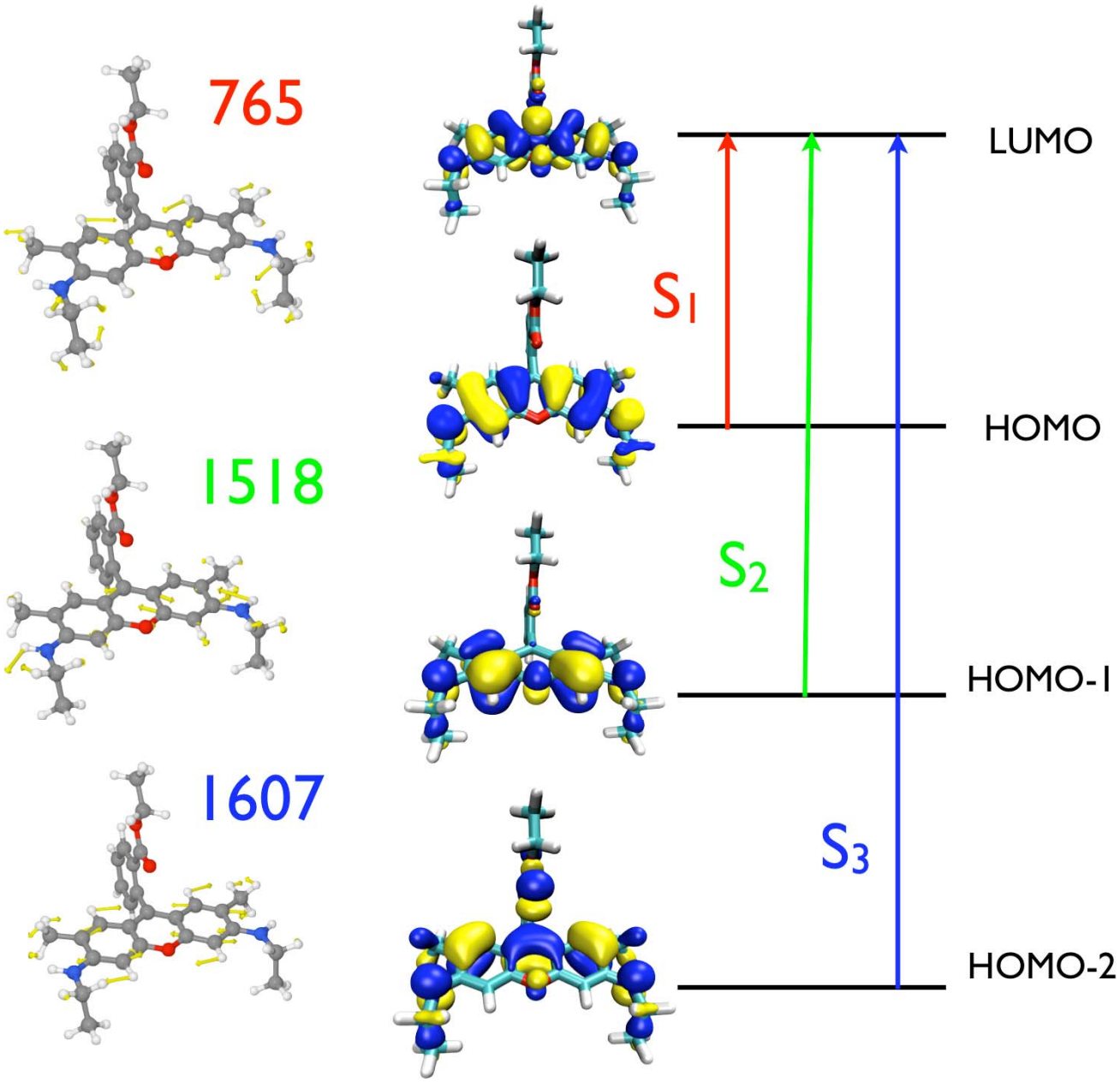


Figure 6. Frontier orbitals involved in the electronic transitions responsible for the features in the one- and two-photon absorption spectra in Figure 5. Normal mode coordinates and frequencies for the vibrations that experience strong resonance enhancement: 765 for S_1, 1518 for S_2, 1607 for S_3. Frequencies given here are from our DFT calculations.

scattering for a molecule the size of R6G is non-trivial and its magnitude is likely to be comparable or smaller than the cross sections obtained for the A-term.

The hyper-Raman spectrum of R6G, therefore, is dominated by a strong off-resonance spectrum for which only a few bands are selectively enhanced by resonance with the different electronic states. This also explains the good agreement between the simulated off-resonance hyper-Raman spectrum compared with the experimental SEHRS spectrum and suggests that the normal approximations made in calculating resonance hyper-Raman scattering are not applicable to the case of R6G. This is in sharp contrast to the resonance Raman spectrum of R6G, which is strongly enhanced for excitations into the S_1 band. The fact that the hyper-Raman spectrum is not strongly dominated by A-term resonance enhancements also explains why it appears very different from the corresponding SERS spectrum, resolving a long standing question as to the origin of the difference in the SERS and SEHRS spectra of R6G.

In this work we have demonstrated the ability of SEHRS to probe, with high sensitivity, a molecular electronic excited state in the R6G molecule which is not accessible via one-photon excitation. Direct comparison with ab initio simulations of the one- and two-photon properties of R6G enabled a detailed understanding of the relevant electronic excited states. We believe that the complementary nature of the hyper-Raman selection rules, when combined with the large surface enhancement factors provided by plasmonic nanostructures, yields a general method to explore the potential energy landscape of “dark” electronic states.

Experimental Section

Citrate reduced Ag colloids were treated with R6G and aggregated with NaCl (~10 mM). The SEHRS measurements were carried out on an inverted microscope using a 20X objective (NA=0.5). A mode-locked Ti:Sapphire (2 ps, 80 MHz) was used as the excitation source. The hyper-Raman scattered light, after passing through an appropriate filter, was dispersed in a grating spectrometer and detected using a CCD camera. All spectra are reported *without* baseline or background corrections. Typical laser powers were ~5 mW (~63 pJ per pulse) at the sample. To check for the influence of R6G dimers, we recorded SEHRS spectra with varying concentrations of R6G (between 10^{-5} and 10^{-10} mol L^{-1}). No changes in the spectral features were observed. (see Supporting Information). We have further checked that the spectra do not change as a function of laser power by recording spectra with excitation energies between 500 μW and 10 mW at the sample.

References for Chapter I

1. Fang, C.; Frontiera, R. R.; Tran, R.; Mathies, R. A. Mapping gfp structure evolution during proton transfer with femtosecond raman spectroscopy. *Nature* **2009,** *462* (7270), 200-U74.
2. Mirkin, C. A.; Ratner, M. A. Molecular electronics. *Annu. Rev. Phys. Chem.* **1992,** *43*, 719-754.
3. Mayer, A. C.; Scully, S. R.; Hardin, B. E.; Rowell, M. W.; McGehee, M. D. Polymer-based solar cells. *Materials Today* 2007**,** *10* (11), 28-33.
4. Myers, A. B., Excited electronic state properties from ground-state resonance raman intensities. In *Laser techniques in chemistry*, Myers, A. B.; Rizzo, T. R., Eds. John Wiley and Sons, Inc.: New York, 1995.
5. Long, D. A., The raman effect: A unified treatment of the theory of raman scattering by molecules. John Wiley & Sons, LTD: 2002.
6. Coe, J. D.; Martinez, T. J. Ab initio multiple spawning dynamics of excited state intramolecular proton transfer: The role of spectroscopically dark states. *Mol. Phys.* 2008**,** *106* (2-4), 537-545.
7. Kelley, A. M. Hyper-raman scattering by molecular vibrations. *Annu. Rev. Phys. Chem.* 2010**,** *61*, 41-61.
8. Baranov, A. V.; Bobovich, Y. S. Higher-order surface-enhanced raman-scattering. *Jetp Lett.* 1982**,** *35* (4), 181-183.
9. Murphy, D. V.; Vonraben, K. U.; Chang, R. K.; Dorain, P. B. Surface-enhanced hyper-Raman scattering from so32- adsorbed on ag powder. *Chem. Phys. Lett.* 1982**,** *85* (1), 43-47.

10. Golab, J. T.; Sprague, J. R.; Carron, K. T.; Schatz, G. C.; Vanduyne, R. P. A surface enhanced hyper-raman scattering study of pyridine adsorbed onto silver - experiment and theory. *J. Chem. Phys.* 1988**,** *88* (12), 7942-7951.
11. Kneipp, K.; Kneipp, H.; Itzkan, I.; Dasari, R. R.; Feld, M. S. Surface-enhanced non-linear raman scattering at the single-molecule level. *Chem. Phys.* 1999**,** *247* (1), 155-162.
12. Hulteen, J. C.; Young, M. A.; Van Duyne, R. P. Surface-enhanced hyper-raman scattering (sehrs) on ag film over nanosphere (fon) electrodes: Surface symmetry of centrosymmetric adsorbates. *Langmuir* 2006**,** *22* (25), 10354-10364.
13. Kneipp, J.; Kneipp, H.; Kneipp, K. Two-photon vibrational spectroscopy for biosciences based on surface-enhanced hyper-raman scattering. *Proc. Nat. Acad. Sci. USA* 2006**,** *103* (46), 17149-17153.
14. Makarov, N. S.; Drobizhev, M.; Rebane, A. Two-photon absorption standards in the 550-1600 nm excitation wavelength range. *Opt. Express* 2008**,** *16* (6), 4029-4047.
15. Xu, C.; Webb, W. W. Measurement of two-photon excitation cross sections of molecular fluorophores with data from 690 to 1050 nm. *J Opt. Soc. Am. B* 1996**,** *13* (3), 481-491.
16. Moskovits, M. Surface-ehanced spectroscopy. *Reviews of Modern Physics* 1985**,** *57* (3), 783-826.
17. Chung, Y. C.; Ziegler, L. D. The vibronic theory of resonance hyper-raman scattering. *J. Chem. Phys.* 1988**,** *88* (12), 7287-7294.

Appendix for Chapter I

I. Fitting of the Experimental SEHRS Spectra

Peak areas were calculated by fitting each spectrum with multiple Lorentzians and a constant baseline. The fit equations' accuracy was determined by monitoring the residual; the lower residual produced the more accurate fit. Once the residuals were optimized, the equations were individually integrated to provide the peak areas. Though not used, width is also reported in the output. Figure 7 shows an example spectrum from 880 nm, with fit data residuals, and sample peak data output.

II. Concentration study

To check for the influence of R6G dimers, we recorded SEHRS spectra with concentrations of Rhodamine 6G between 10^{-5} and 10^{-10} mol L^{-1}. No changes in the spectral features were observed, except for a decrease in signal at lower concentrations. The spectra reported in Figure 5 were taken at a concentration of 10^{-7} M; however, we have recorded spectra with concentrations as low as 10^{-10} M R6G. Figure 8 shows a spectrum taken with a Rhodamine 6G concentration of 10^{-10} M at 880 nm.

III. Theoretical Methods

In the time-dependent formalism the one-photon absorption (OPA) cross section is given by[1]

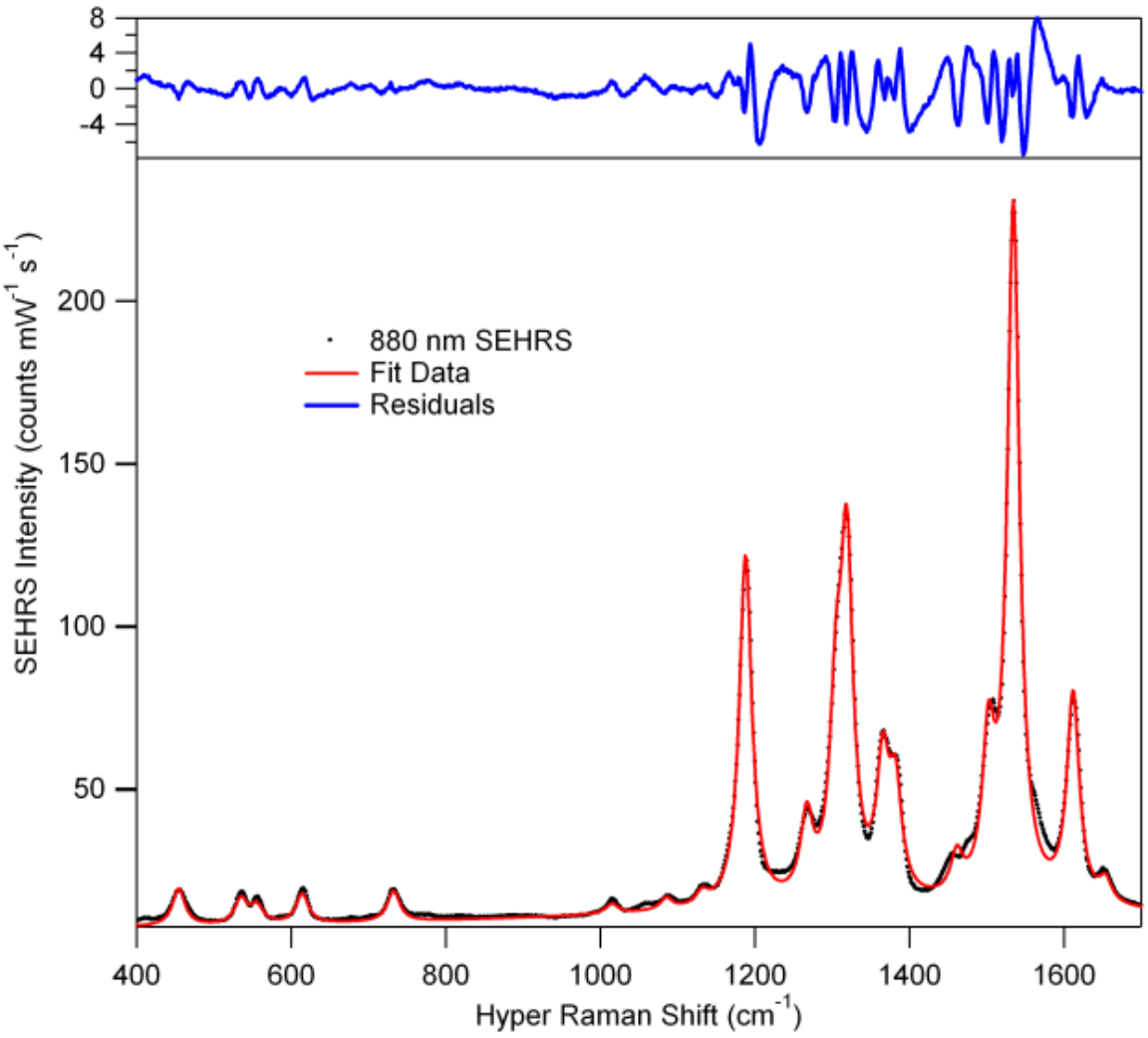


Figure 7. Comparison of the experimental and fitted spectrum obtained for λ_{ex} = 880 nm.

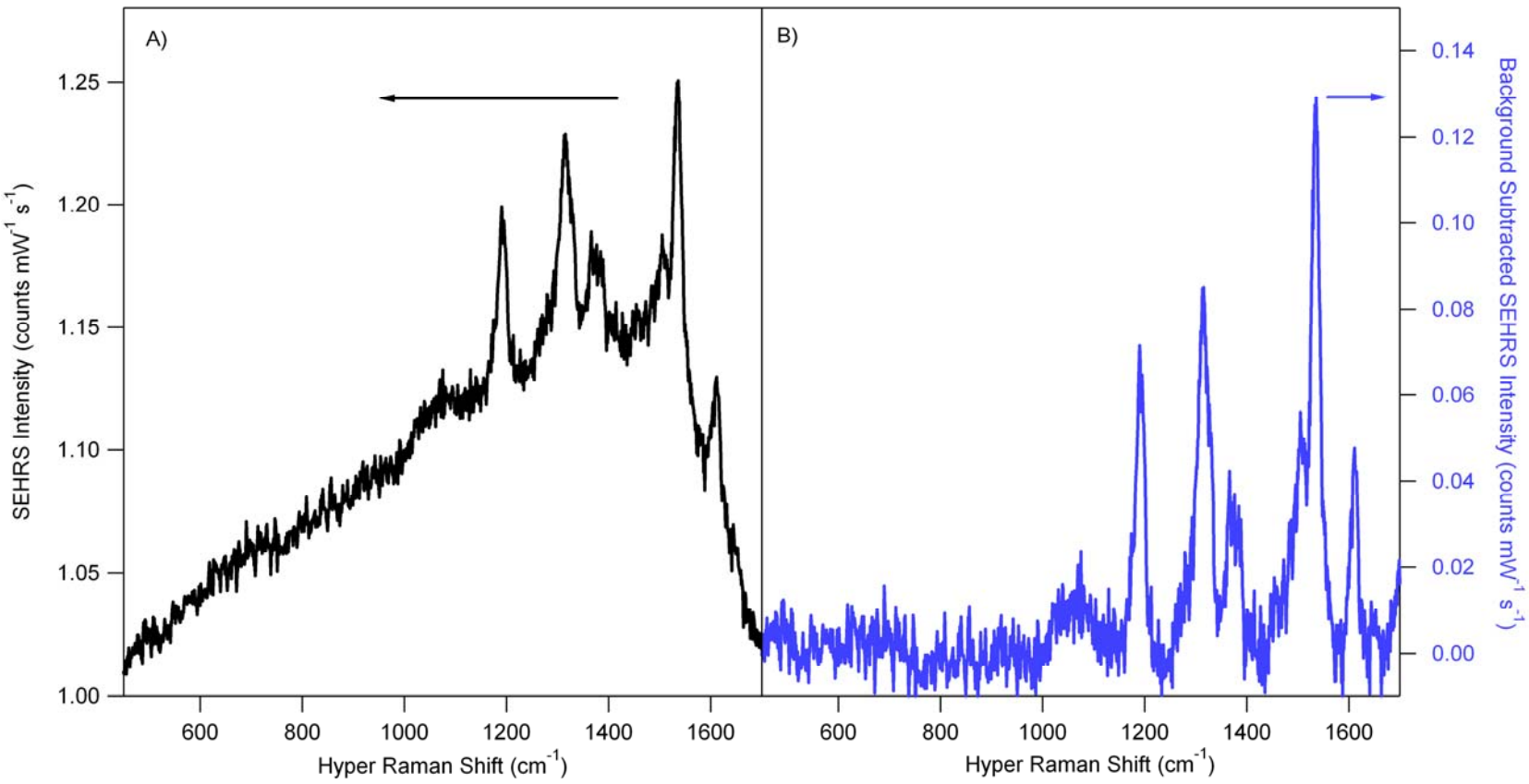


Figure 8. SEHRS of R6G on Ag [R6G]=10^{-10} M at 880 nm. Raw data (left) and baseline corrected data (right).

$$\sigma_{OPA} = \frac{4\pi}{3\hbar c} E_L \sum_n (\mu^{0n})^2 \times \mathrm{Re} \int_0^\infty \langle i | i_n(t) \rangle e^{i(E_L + \nu_{i0})t - \Gamma_n t - (1/2)\Theta^2 t^2} dt$$

where E_L is the energy of the incident light, n the electronic state, μ^{0n} the electronic transition dipole moment, vi0 the vibrational energy of state |i>, and |in(t)> is the wavepacket corresponding to the time-dependent nuclear wavefunction of electronic state n. The homogeneous broadening is treated phenomenologically using Δn, and inhomogeneous broadening using r. The overlap between the initial and final wavepacket can be obtained analytically using the independent mode displaced harmonic oscillator (IMDHO) method[2]

In a similar way we can write the two-photon absorption (TPA) cross section as

$$\sigma_{TPA} = \left(\frac{8\pi^3 \alpha^2 \hbar^3}{e^4} \right) \omega^2 \sum_n 2 \sum_{\alpha\beta} \left[S^n_{\alpha\alpha} S^n_{\beta\beta} + S^n_{\alpha\beta} S^n_{\alpha\beta} + S^n_{\alpha\beta} S^n_{\beta\alpha} \right]$$
$$\times \mathrm{Re} \int_0^\infty \langle i | i_n(t) \rangle e^{i(2E_L + \nu_{i0})t - \Gamma_n t - (1/2)\Theta^2 t^2} dt$$

where $S_{\alpha\beta}$ are the two-photon transition matrix elements and $\hbar\omega$ is the photon energy.

The ground state equilibrium geometry and normal modes for the R6G complexes was determined using the B3LYP functional and 6-311G* basis set. Optical properties needed for simulating OPA, including the excited state energies used for determining the dimensionless displacements, were calculated using the TDDFT linear response method in NWChem.[3] The two-photon

transition matrix elements were calculated using quadratic response theory as implemented in the Dalton program.[4]

Simulation parameters for the OPA and TPA spectrum were determined by shifting the peak position and changing the peak width to match the experimental absorbance spectrum using a mixture of homogeneous and inhomogeneous broadening. Peak height was normalized to match the experimental absorbance spectrum by applying a scale factor to the DFT results. This accounts for lack of solvent effects in the calculations and shortcomings in the XC-potential used.

The following parameters were used to simulate the OPA spectrum: Γ_{S1}=500cm^{-1}, Γ_{S2}=1400cm^{-1}, Γ_{S3}=625 cm^{-1}, Θ = 0 cm^{-1}, and a scale factor of 1.59. For the TPA spectrum we used: Γ_{S1}=600cm^{-1}, Γ_{S2}=400cm^{-1}, Γ_{S3}=550 cm^{-1}, Θ = 0 cm^{-1}, and a scale factor of 37.9. We also found that it was necessary to scale the S2 state two-photon transition moment by an additional factor of 1.5.

The differential hyper-Raman scattering cross section is given by[5]

$$\frac{d\sigma}{d\Omega} = \frac{16\pi^2 h^3 \alpha^3 \nu_s^4 P_i}{Nc^2 e^6} \left\langle \beta_{\alpha\beta\gamma} \right\rangle^2$$

where α is the fine structure constant, ν_s is the frequency of the scattered radiation, P_i is the population of the initial vibrational state, N is the number of scatters per unit volume, h is Planck's constant, c is the speed of light, and $\beta_{\alpha\beta\gamma}$ is the hyperpolarizability. The < > indicates that the hyperpolarizability tensors were

obtained assuming averaging over all orientations of the molecule with respect to the incident light.[6]

In the time-dependent theory the A-term hyperpolarizability is given by[7]

$$\beta_{\alpha\beta\gamma} = \sum_n \mu_\alpha^{0n} S_{\beta\gamma}^{0n} \times i\int_0^\infty \langle f \,|\, i_n(t)\rangle e^{i(2E_L+\nu_{i0})t-\Gamma_n t-(1/2)\Theta^2 t^2}\, dt$$

The hyper-Raman cross section on resonance with S_1, S_2, and S_3 were simulated using the same parameters needed for the TPA spectra. However, we did not include the scale factors when simulating the cross sections.

Alternatively, away from strong resonances the hyperpolarizability can be written using geometric derivatives of the electronic hyperpolarizability as[6]

$$\beta_{\alpha\beta\gamma} = b_{\nu_a}\beta_{\alpha\beta\gamma} = \sqrt{\frac{h}{8\pi^2 c\,\nu_a}}\frac{\partial\beta_{\alpha\beta\gamma}^{el}}{\partial Q_a}$$

where Q_a is the normal mode with vibrational frequency ν_a. The hyperpolarizability derivatives needed to simulate the off-resonance hyper-Raman spectrum were calculated from using three-point finite-differentiation of the static hyperpolarizability. These calculations were done using the response module of the ADF program.[8] We used the BP86 XC-functional and a TZP basis set.

IV. Comparison of Theory and Experiment

To understand in more detail the SEHRS spectra of R6G we calculated the off-resonance hyper-Raman spectra using TDDFT. The comparison between the simulated off-resonance spectrum with the experimental SEHRS spectrum obtained at 1050 nm is presented in Figure 9. Overall we see that there is a good agreement between the simulated and measured spectra, both with respect to band positions and intensities. However, there are some noticeable differences between the simulated spectra and that measured experimentally. For example, in the simulations, the 1315 band is the strongest whereas experimentally it is the band at 1535. This is most likely due to the neglect of surface and resonance effects in the simulations. Despite these differences, the good agreement enabled a detailed assignment of the experimental spectrum. As we discuss in the manuscript the good agreement results because the hyper-Raman spectrum of R6G is dominated by the off-resonance spectrum.

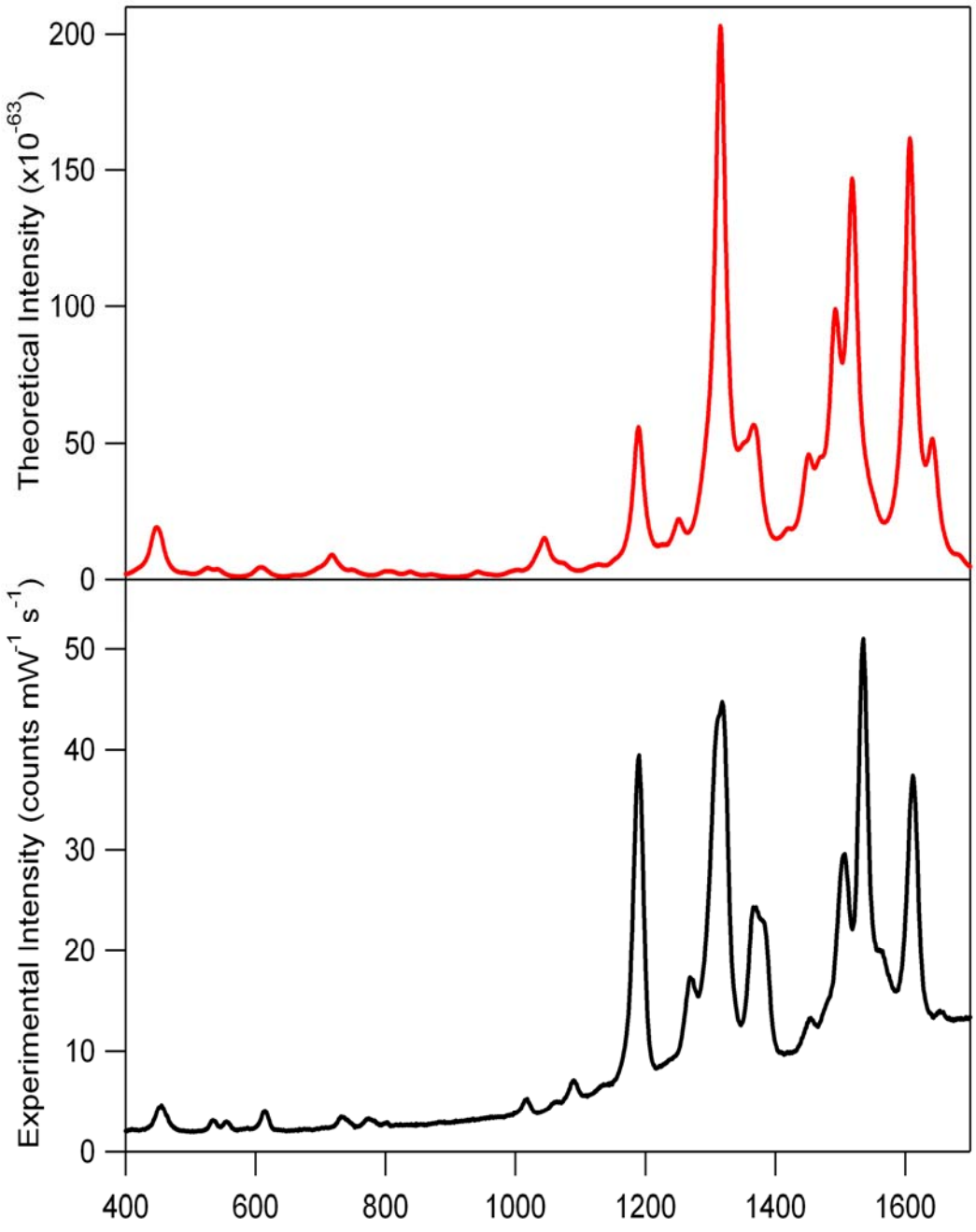


Figure 9. Simulated off-resonance hyper-Raman spectrum (top) and experimental SEHRS spectrum obtained at 1050 nm (bottom).

V. References for Appendix

1 Tannor, D. J.; Heller, E. J. J. Chem. Phys. **1982**, 77, 202

2 Neese, F.; Petrenko, T.; Ganyushin, D.; Olbrich, G. Coord. Chem. Rev. **2007**, 251, 288

3 Bylaska, E. J. et al., NWCHEM, A computational chemistry package for parallel computers, Version 5.1, Pacific Northwest National Laboratory, Richland, Washington 99352-0999, USA, **2007** (a modified version).

4 DALTON, a molecular electronic structure program, Release 2.0 (**2005**), see http://daltonprogram.org/

5 Ziegler, L. D. J. Raman Spec. **1990**, 21, 769–779

6 Quinet, O.; Champagne, B.; Gisbergen, S. J. A. V. Int. J. Quant. Chem. **2005**, 106, 599–608

7 Shoute, L. C. T.; Bartholomew, G. P.; Bazan, G. C.; Kelley, A. M. J. Chem. Phys., **2005**, 122, 184508

8 Baerends, E. J. et al. Amsterdam Density Functional. http://www.scm.com

CHAPTER II

PROBING TWO-PHOTON PROPERTIES OF MOLECULES: LARGE NON-CONDON EFFECTS DOMINATE THE RESONANCE HYPER-RAMAN SCATTERING OF RHODAMINE 6G

A version of this chapter was originally published by Chris B. Milojevich, Daniel W. Silverstein, Lasse Jensen, and Jon P. Camden.

Chris B. Milojevich, Daniel W. Silverstein, Lasse Jensen, and Jon P. Camden. **Probing Two-Photon Properties of Molecules: Large Non-Condon Effects Dominate the Resonance Hyper-Raman Scattering of Rhodamine 6G**. *Journal of the American Chemical Society* 2011 133 (37), 14590-14592.

The article is represented in the form which it was published, with the exception that the following JACS required sections have been removed: Acknowledgements, Associated Content, and Author Information. The supplemental information section of the paper has been added as an appendix. The dissertation author conducted all of the experiments indicated in the paper, designed each of the figures, and wrote the experimental portion of the appendix. The calculations indicated in the paper were conducted by DW Silverstein and L Jensen. All authors contributed equally and approved the final document.

Abstract

Experimentally measured resonance hyper-Raman spectra spanning the $S_1 \leftarrow S_0$, $S_2 \leftarrow S_0$, and $S_3 \leftarrow S_0$ transitions in Rhodamine 6G are recorded. These spectra are compared to first-principles calculations of the resonance hyper-Raman intensity which include both Franck-Condon (A-term) and non-Condon (B-term) scattering effects. Excellent agreement is observed between the experimental and theoretical calculations demonstrating that first-principles calculation of

hyper-Raman intensities are now possible for large molecules such as R6G. Such agreement indicates that resonance hyper-Raman will now be a routine aid for probing multiphoton processes. This work further shows that optimization of molecular properties to enhance either A- or B-term scattering might yield molecules with significantly enhanced two-photon properties.

Published Work

There is significant interest in utilizing multi-photon processes for applications in all-optical switching, energy-up conversion, and biological imaging.[1-4] For example, two-photon transitions can be used in optical power limiting materials, photodynamic therapy, optical data storage, two-photon fluorescence microscopy, and two-photon photopolymerization for 3D lithographic microfabrication.[2-7] Two-photon techniques also provide a method to probe "dark" electronic states, i.e. those which are either forbidden or only weakly allowed via one-photon excitation.[8]

Hyper-Raman scattering[9] is a type of non-linear light scattering in which a photon at $\omega=2\omega_0-\omega_v$ is incoherently scattered, where ω_0 is the laser frequency and ω_v is a vibration characteristic of the material. Resonance hyper-Raman (RHR) scattering provides detailed information about the geometry of two-photon accessible excited states. For weakly allowed one- or two-photon transitions resonance hyper-Raman scattering provides additional information about non-Condon effects, i.e. the nuclear dependence of the one- or two-photon transition moments. The framework provided by the vibronic theory of resonance hyper-

Raman[10] interprets the observed scattering intensities in terms of vibronic coupling terms, Franck-Condon factors, and one- and two-photon dipole moments and their nuclear dependence. This rich set of information, however, is not easily interpreted due to the complex interplay of the various excited states and their topology.

In this communication we report a detailed comparison of experimentally measured and theoretically calculated resonance hyper-Raman intensities spanning the $S_1 \leftarrow S_0$, $S_2 \leftarrow S_0$, and $S_3 \leftarrow S_0$ transitions in Rhodamine 6G (R6G). This comparison allows us to identify and to quantify the various contributions to the resonance hyper-Raman intensities and demonstrates that reliable calculations of resonance hyper-Raman spectra including both Franck-Condon and non-Condon effects are now possible for large molecules such as R6G. Furthermore, we find that the hyper-Raman scattering of R6G is dominated by non-Condon effects and that interference between the two lowest electronic states plays an essential role, even though they are separated by more than 100 nm (~0.4 eV).

Surface enhanced hyper-Raman spectra (SEHRS) of R6G adsorbed on aggregated silver colloids were recorded for excitation wavelengths spanning the two-photon absorption spectrum of R6G. The concentration of R6G was 10^{-7} M and the laser bandwidth was narrowed, in comparison to our previous studies,[8] by increasing the pulse length to ~6ps. While hyper-Raman scattering is an inherently weak process, the signal originating from molecules located near the

surface of a plasmonic nanostructure can be enhanced by many orders of magnitude;[11-14] therefore, extending the utility of hyper-Raman to wide a range of chromophores.

Figure 10 displays the resonance hyper-Raman spectrum (Figure 10a) and the SEHRS spectra (Figure 10b) of R6G at λ=825 nm. While there are minor differences between the RHR and SEHRS spectra, the good agreement suggests that surface effects are a minor perturbation on the spectra. Figure 10 also compares the experiment with first-principles simulations using a time-dependent formalism for describing the resonance hyper-Raman scattering. The molecular properties needed for simulating the hyper-Raman scattering were obtained using time-dependent density-functional theory (TDDFT) using B3LYP/6-311G*. Details of the simulations are provided in the Supporting Information. Our simulations included the three lowest excited states (S_1,S_2, and S_3) and explored Franck-Condon (A-term) and non-Condon (B-term) scattering effects.

Good agreement between theory and experiment is obtained when both A- and B-term scattering is included (Figure 10a, b, and c). The spectra calculated using only Franck-Condon effects (Figure 10d) does not agree with experiment although, as expected, it appears similar to the resonance Raman spectra of R6G. A further comparison of experimental and theoretical spectra for wavelengths spanning the S_1, S_2, and S_3 transitions are displayed in Figure 11. To the best of our knowledge this represents the first first-principles calculation of

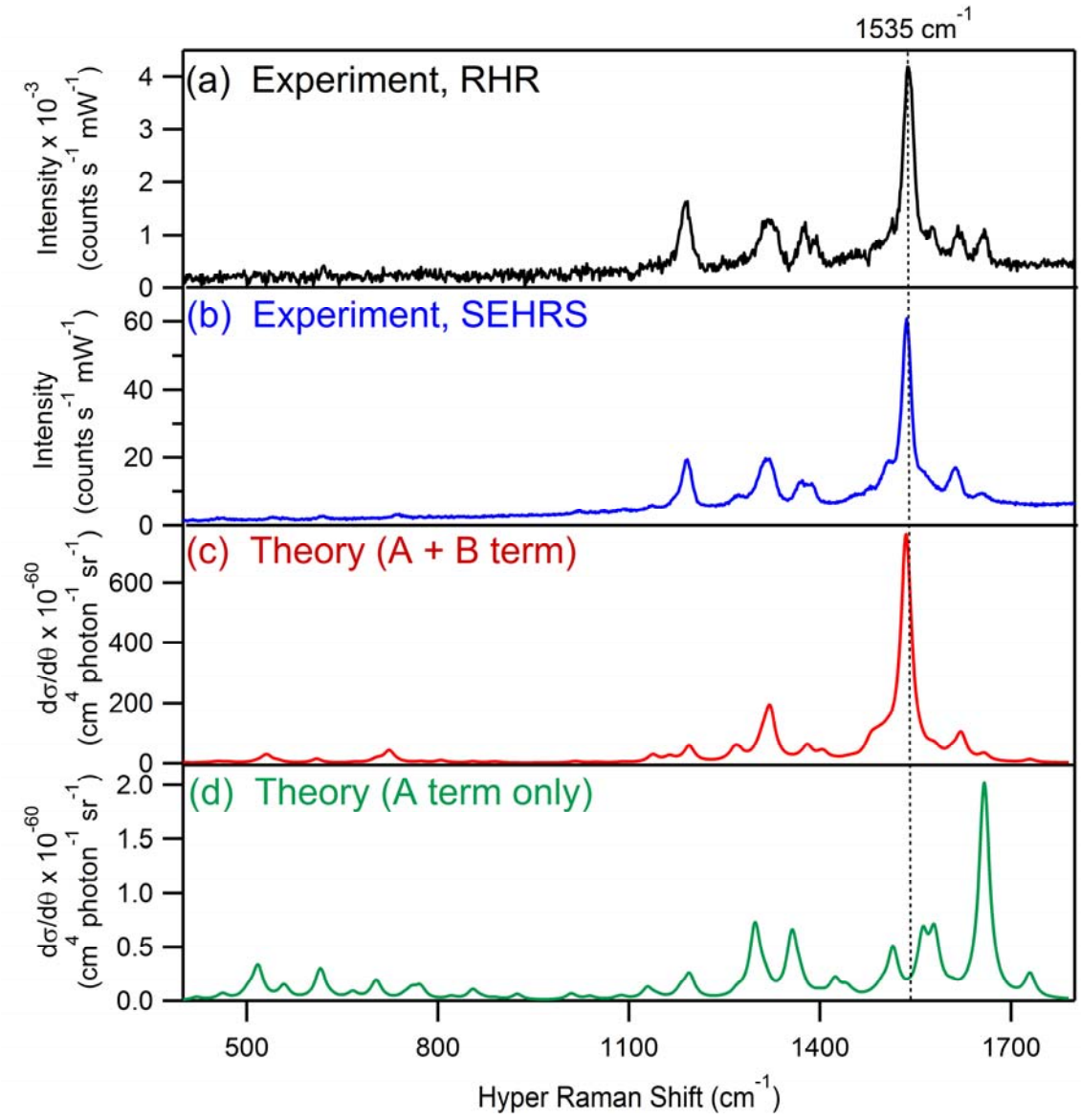


Figure 10. Comparison of experimentally measured and theoretically calculated resonance hyper-Raman spectra of R6G at λ=825nm. (a) Resonance hyper-Raman of 10^{-3} M R6G in water, (b) SEHRS of R6G on aggregated silver colloids, (c) TDDFT calculation of the RHR spectrum including both Condon (A-term) and non-Condon (B-term) scattering, (d) calculations including only A-term scattering. The spectra are measured and calculated on resonance with the two photon $S_2 \leftarrow S_0$ transition.

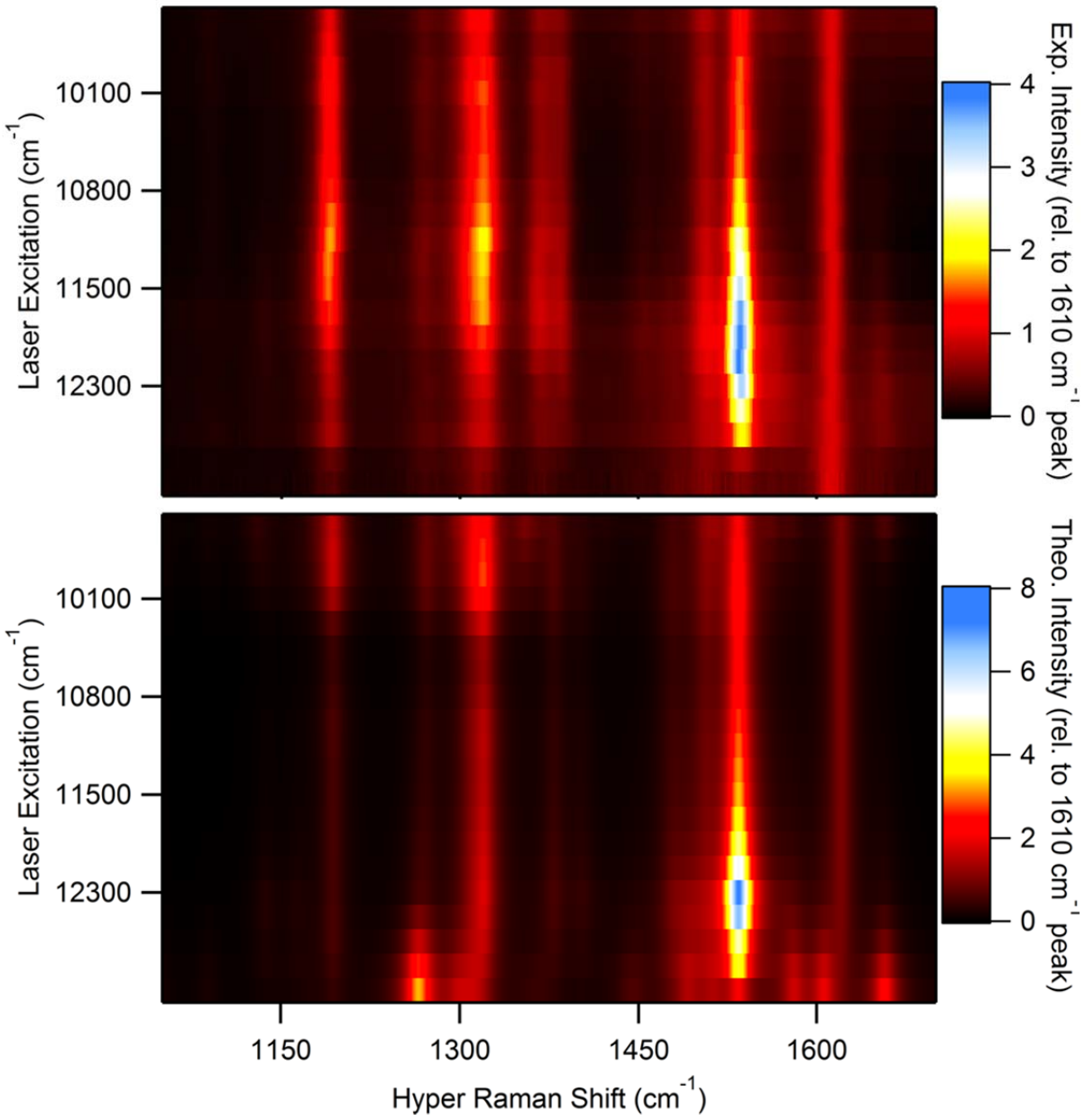


Figure 11. Comparison of experimentally measured and theoretically calculated hyper-Raman spectra of R6G for excitation wavelengths between 750 and 1050 nm. An asterisk (*) indicates the 1535 cm^{-1} peak.

RHR intensities, including non-Condon effects, for a molecule as large as R6G. SEHRS spectra are used for this comparison as the large two-photon excited fluorescence of R6G overwhelms the unenhanced RHR signal of R6G without the fluorescence quenching provided by the Ag nanoparticles. The spectrum shown at λ=825nm (Figure 10) is obtained in the small region where the two-photon fluorescence is minimized.

We now interpret these effects with reference to the one- and two-photon absorption spectrum of R6G shown in Figure 12. In a previous publication[8] we found that the dominant 1535 cm^{-1} band is correlated with the S_2-S_0 transition. The $S_2 \leftarrow S_0$ transition is two-photon, but only *weakly* one-photon allowed; therefore, the non-Condon effects arise from the nuclear dependence of the transition dipole moment (B_1-term). In contrast $S_1 \leftarrow S_0$ is strongly one-photon allowed but only weakly two-photon allowed; therefore, on resonance with S_1 the non-Condon effects arise from the nuclear dependence of the two-photon transition moments (B_2-term) Figure 13compares B_2 and B_1 terms for the two states and displays the normal mode associated with the strongest vibrational band (1535 cm^{-1}) observed on resonance with S_2. From this data we must conclude that the hyper-Raman spectrum of R6G is characterized by significant non-Condon effects for both the S_1 and the S_2 states.

Non-Condon scattering is typically weak since either the two-photon or the one-photon electronic transition is forbidden (or nearly so). Our simulations show, however, that R6G has a large differential hyper-Raman cross section of 7.6x10^{-}

^{58} cm^4 s photon^{-1} sr^{-1} on resonance with the S_2 state. At this wavelength the contribution from the B-term is about 300 times stronger than the contribution from the A-term. For comparison the hyper-Raman differential cross section of p-nitroaniline (PNA), a prototypical push-pull molecule with a significant hyperpolarizability, is only 4.1x10^{-58} cm^4 s photon^{-1} sr^{-1} on resonance with a state that is *both* one and two-photon allowed. This suggests that further optimization of molecular properties to enhance either A- or B-term scattering could yield molecules with significantly larger hyper-Raman cross-sections.

In resonance Raman scattering it is well known that interference effects in the spectrum may arise if multiple excited states contribute to the scattering process. This typically requires spectral overlap between the excited states as the Franck–Condon scattering intensity falls off rapidly with detuning from resonance. This is *not* the case, however, for B-term scattering and our calculations show significant interference between the two lowest excited states in the RHR spectra even though they are separated by more than 100 nm. On resonance with S_2 we find that the constructive interference between S_2 and S_1 state amounts to roughly 34% the intensity while contributions from only S_2 or S_1 contribute 53% and 13% respectively. While the interference is constructive when resonant with S_2 we find that it is destructive when resonant with S_1.

For the S_2 state we find that the two-photon transition moment (S_{20}) and the nuclear dependence of the transition moment ($d\mu_{20}/dQ$) are almost anti-parallel. Likewise for the S_1 state the one-photon transition moment (μ_{10}) and the nuclear

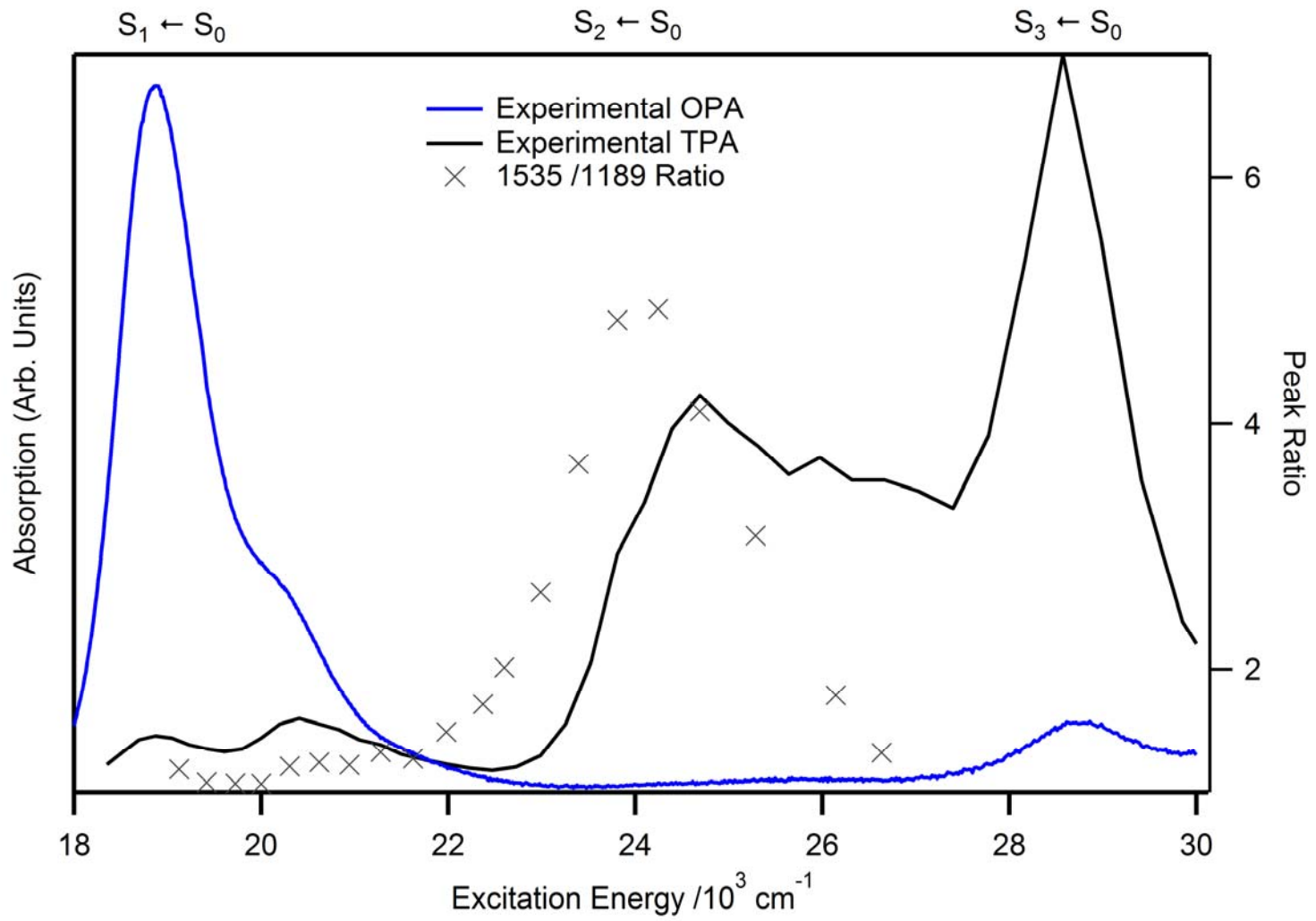


Figure 12. Comparison of the experimentally measured[15] and theoretically calculated (this work) two-photon absorption spectra of R6G. The ratio of the 1535 cm^{-1} to 1189 cm^{-1} peaks is reproduced from Ref. 8.

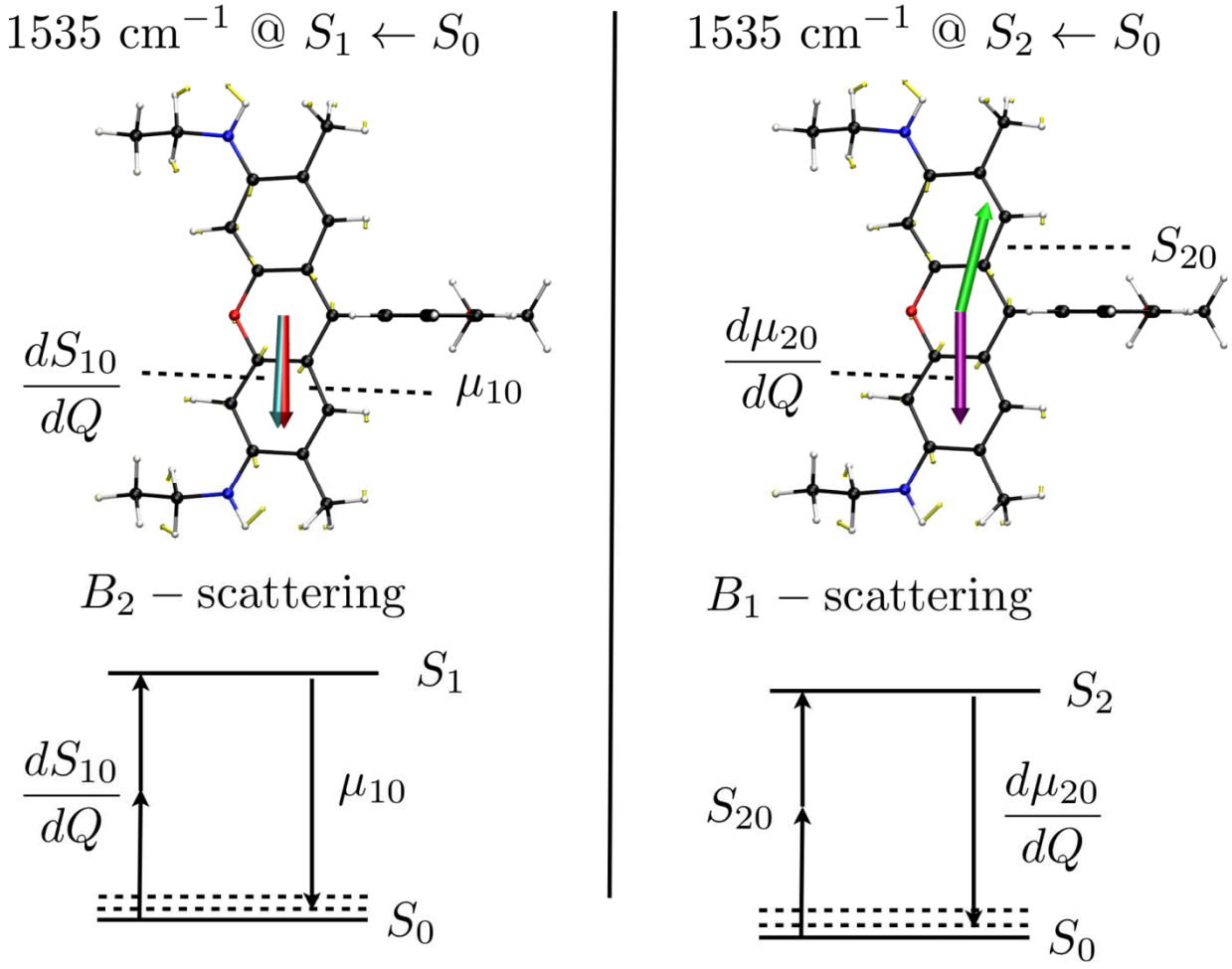


Figure 13. Non-Condon effects in R6G. The hyper-Raman scattering resonant with the S_1 state is dominated by B_2-scattering where the non-Condon effects is due to the nuclear dependence of the two-photon transition moment. For the S_2 state the hyper-Raman scattering is dominated by non-Condon effects in the one-photon transition moment, B_1 scattering. Depicted for the two electronic states are the normal mode of the 1535cm^{-1} vibration and the corresponding one- and two-photon transition moments.

dependence of the two-photon transition moment (dS_{10}/dQ) are parallel. In the case of S_1 this leads to destructive interference, whereas in the case of S_2 it leads to constructive interference.

This work demonstrates that the complex interplay of electronic excited states encountered in resonance hyper-Raman is now accessible using first-principles theory for large molecules such as R6G. This agreement was achieved only after the inclusion of non-Condon terms in the theory, which yields important insights into the two-photon properties of the molecular chromophore. Further, this work suggests that non-Condon terms and interference effects are more important in determining two-photon properties than previously expected. Future studies utilizing resonance hyper-Raman and SEHRS will elucidate the complex interplay of electronic excited states encountered in multi-photon processes such as all-optical switching, energy up-conversion, and biological imaging.

References for Chapter II

1. Hales, J. M.; Matichak, J.; Barlow, S.; Ohira, S.; Yesudas, K.; Bredas, J. L.; Perry, J. W.; Marder, S. R. *Science* **2010**, *327*, 1485.
2. He, G. S.; Tan, L. S.; Zheng, Q.; Prasad, P. N. *Chemical Reviews* **2008**, *108*, 1245.
3. Pawlicki, M.; Collins, H. A.; Denning, R. G.; Anderson, H. L. *Angewandte Chemie-International Edition* **2009**, *48*, 3244.
4. So, P. T. C.; Dong, C. Y.; Masters, B. R.; Berland, K. M. *Annual Review of Biomedical Engineering* **2000**, *2*, 399.
5. Cumpston, B. H.; Ananthavel, S. P.; Barlow, S.; Dyer, D. L.; Ehrlich, J. E.; Erskine, L. L.; Heikal, A. A.; Kuebler, S. M.; Lee, I. Y. S.; McCord-Maughon, D.; Qin, J. Q.; Rockel, H.; Rumi, M.; Wu, X. L.; Marder, S. R.; Perry, J. W. *Nature* **1999**, *398*, 51.
6. Kawata, S.; Kawata, Y. *Chemical Reviews* **2000**, *100*, 1777.
7. Larson, D. R.; Zipfel, W. R.; Williams, R. M.; Clark, S. W.; Bruchez, M. P.; Wise, F. W.; Webb, W. W. *Science* **2003**, *300*, 1434.
8. Milojevich, C. B.; Silverstein, D. W.; Jensen, L.; Camden, J. P. *ChemPhysChem* **2011**, *12*, 101.
9. Kelley, A. M. *Annu. Rev. Phys. Chem.* **2010**, *61*, 41.
10. Chung, Y. C.; Ziegler, L. D. *J. Chem. Phys.* **1988**, *88*, 7287.
11. Baranov, A. V.; Bobovich, Y. S. *JETP Letters* **1982**, *35*, 181.
12. Golab, J. T.; Sprague, J. R.; Carron, K. T.; Schatz, G. C.; Van Duyne, R. P. *J. Chem. Phys.* **1988**, *88*, 7942.

13. Kneipp, K.; Kneipp, H.; Itzkan, I.; Dasari, R. R.; Feld, M. S. *Chem. Phys.* **1999**, *247*, 155.
14. Murphy, D. V.; Vonraben, K. U.; Chang, R. K.; Dorain, P. B. *Chem. Phys. Lett.* **1982**, *85*, 43.
15. Makarov, N. S.; Drobizhev, M.; Rebane, A. *Optics Express* **2008**, *16*, 4029.

Chapter II Appendix

I. Experimental Methods

Experimental Set-up

The Raman and hyper-Raman experiments were carried out with a Ti:sapphire laser (Tsunami, Spectra-Physics) that is pumped with a 532 nm Nd:YAG laser (Millenium XV, Spectra-Physics). The wavelength range of the Ti:sapphire is 690 – 1050 nm, and it generates a 5 ps pulse (as measured with an autocorrelator) at a rate of 81 MHz. For most wavelengths, the output can be modulated between 0.3 and 3 Watts using a half-wave plate and Glan polarizer (Thorlabs). Vertical polarization is then doubled in a frequency doubler (Spectra-Physics), and the horizontal polarization is converted to vertical polarization with a periscope before it is used to excite the sample. The beam is then sent into an inverted microscope (Ti-U, Nikon) where a dichroic mirror reflects the excitation beam through any of two objectives (20x or 60x) which is focused on the sample. The objective collects the back-scattered light, transmitting it through the dichroic, and then either through the eyepiece, a NIR camera (UM-300, Uniq Vision), or to a spectrometer (Acton, Princeton Instruments) with a back-lit CCD LN-cooled detector (PIXIS 100, Princeton Instruments). The Raman spectrum of liquid cyclohexane was used to calibrate the spectrometer at 440 nm, and this calibration was used to set the calibration of rhodamine 6G at a 880 nm exitation.

Nanoparticle cluster synthesis

Silver nanoparticles are synthesized using the citrate reduction method specified by Lee and Meisel [S1]. Specifically, nanoparticles were experimentally determined to be SEHRS active when both the silver nitrate and sodium citrate are at the same concentration (1×10^{-3} M) when creating the nanoparticles. The nanoparticle extinction spectrum has a maximum at 498 nm.

RHR measurements

For the solution hyper-Raman measurements, an aqueous solution of rhodamine 6G is prepared at 10^{-4} M. This solution was placed in a quartz cuvette, into which 0.5 W of 825 nm light was focused through a 60x objective (Nikon, NA = 0.8). Total acquisition time is 60 minutes.

SEHRS measurements

Rhodamine 6G is added to the nanoparticle sample at a concentration of about 10^{-7} M, unless specified otherwise. After approximately one hour, a small amount of sodium chloride solution (0.1 M) is added to the colloids to force them to aggregate. Immediately after adding the sodium chloride, the colloids change to a darker color and 24 hours after the addition all of the aggregates precipitate out of solution. With agitation, the nanoparticles continue to aggregate into “clusters” which are large enough to see with the naked eye. For the SEHRS measurements, ~3 mW of 825 nm radiation

is focused through a 20x objective (Nikon, NA = 0.5) on a single nanoparticle cluster. The total acquisition time is 120 seconds.

II. Theoretical Methods

The theoretical spectra were simulated using the time-dependent formalism for spectroscopy. [1,2,5,6] The two-photon absorption cross section is given by

$$\sigma_{TPA}^{FC}(\omega) = \left(\frac{4\pi^3 \alpha^2 \omega^2 \hbar^3}{e^4} \right) \sum_k \delta_{TPA}^{0k} \, \mathrm{Re} \int_0^\infty \left\langle I_0 \middle| I_k(t) \right\rangle e^{i(\varepsilon_{I_0} + 2\omega)t - \Gamma_k t} \, dt$$

for the Franck-Condon term,

$$\sigma_{TPA}^{FC-HT}(\omega) = \left(\frac{4\pi^3 \alpha^2 \omega^2 \hbar^3}{e^4} \right) \sum_{k,a} (\delta_{TPA}^{0k})^{a'} \sqrt{\frac{\hbar}{2\omega_a}} \times \mathrm{Re} \int_0^\infty \sqrt{I_a + 1} \left\langle (I_a + 1)_0 \middle| I_k(t) \right\rangle e^{i(\varepsilon_{I_0} + 2\omega)t - \Gamma_k t} dt$$

for the Frank-Condon/Herzberg-Teller interference term, and,

$$\sigma_{TPA}^{HT}(\omega) = \left(\frac{4\pi^3 \alpha^2 \omega^2 \hbar^3}{e^4} \right) \sum_{k,a,b} (\delta_{TPA}^{0k})^{ab'} \sqrt{\frac{\hbar}{2\omega_a}} \sqrt{\frac{\hbar}{2\omega_b}} \times \mathrm{Re} \int_0^\infty \left\langle (I_a + 1)_0 \middle| (I_b + 1)_k(t) \right\rangle e^{i(\varepsilon_{I_0} + 2\omega)t - \Gamma_k t} dt$$

for the Herzberg-Teller term.

Similarly the resonance hyper-Raman scattering is given by

$$A = \sum_{k} (\mu_{\alpha}^{0k})^{eq} (S_{\beta\gamma}^{0k})^{eq} \times i \int_{0}^{\infty} \left\langle F_0 \middle| I_k(t) \right\rangle e^{i(\varepsilon_{I_0} + 2\omega)t - \Gamma_n t} \, dt$$

for the A-term

$$B_1 = \sum_{k,a} \sqrt{\frac{\hbar}{2\omega_a}} (\mu_{\alpha}^{0k})^{a'} (S_{\beta\gamma}^{0k})^{eq} \times$$
$$i \int_{0}^{\infty} (\sqrt{F_a} \left\langle (F_a - 1)_0 \middle| I_k(t) \right\rangle + \sqrt{F_a + 1} \left\langle (F_a + 1)_0 \middle| I_k(t) \right\rangle) e^{i(\varepsilon_{I_0} + 2\omega)t - \Gamma_n t} dt$$

for the B_1 term, and,

$$B_2 = \sum_{k,b} \sqrt{\frac{\hbar}{2\omega_b}} (\mu_{\alpha}^{0k})^{eq} (S_{\beta\gamma}^{0k})^{b'} \times i \int_{0}^{\infty} \sqrt{I_b + 1} \left\langle F_0 \middle| (I_b + 1)_k(t) \right\rangle e^{i(\varepsilon_{I_0} + 2\omega)t - \Gamma_n t} \, dt$$

for the B_2 term.

In the above equations $\hbar\omega$ is the photon energy of the incident light, k the excited electronic state, μ^{0k} the electronic transition dipole moment, δ_{tpa} the two-photon transition strength , $S_{\beta\gamma}$ the two-photon transition moments, ε_{I0} the vibrational energy of state |I>, and |Ik(t)> is the wavepacket corresponding to the time-dependent nuclear wavefunction of electronic state k. The two-photon absorption cross sections depend on the fine structure constant α and fundamental charge *e*. In the Herzberg-Teller/B terms, ω_n is the normal mode frequency for mode Q_n. The homogeneous broadening is

treated phenomenologically using Γ_n. The notations $(A)^{eq}$ and $(A)^{a'}$ indicate the property A is evaluated at the ground state equilibrium geometry and derivative of the property along mode Q_a, respectively. The overlap between the initial and final wavepacket can be obtained analytically using the independent mode displaced harmonic oscillator (IMDHO) method.[2]

The ground state equilibrium geometry and normal modes for the R6G complexes was determined using the B3LYP functional and 6-311G* basis set in NWChem.[3] Optical properties needed for simulating TPA and the resonance hyper-Raman scattering were calculated using linear and quadratic response theory as implemented in the Dalton program.[4]

Simulation parameters for the OPA and TPA spectrum were determined by shifting the peak position and changing the peak width to match the experimental absorbance spectrum using a mixture of homogeneous and inhomogeneous broadening. Peak height was normalized for the S_3 state to match the experimental absorbance spectrum by applying a scale factor to the DFT results. This accounts for lack of solvent effects in the calculations and shortcomings in the XC-potential used.

The following parameters were used to simulate the TPA and resonance hyper-Raman spectra: Γ_{S1}=600cm^{-1}, Γ_{S2}=400cm^{-1}, Γ_{S3}=550 cm^{-1}, Θ = 0 cm^{-1} (no inhomogeneous broadening), and a scale factor of 1.59.

References for Appendix

1. Tannor, D. J.; Heller, E. J. J. Chem. Phys. **1982**, 77, 202
2. Neese, F.; Petrenko, T.; Ganyushin, D.; Olbrich, G. Coord. Chem. Rev. **2007**, 251, 288
3. Bylaska, E. J. et al., NWCHEM, A computational chemistry package for parallel computers, Version 5.1, Pacific Northwest National Laboratory, Richland, Washington 99352-0999, USA, **2007** (a modified version).
4. DALTON, a molecular electronic structure program, Release 2.0 (**2005**), see http://daltonprogram.org/
5. Shoute, L. C. T.; Bartholomew, G. P.; Bazan, G. C.; Kelley, A. M. J. Chem. Phys., **2005**, 122, 184508
6. Silverstein, D. W., Jensen, L. , In preparation, **2011**

CHAPTER III

SURFACE-ENHANCED HYPER-RAMAN SCATTERING ELUCIDATES THE TWO-PHOTON ABSORPTION SPECTRUM OF RHODAMINE 6G

A version of this chapter was originally published by Chris B. Milojevich, Daniel W. Silverstein, Lasse Jensen, and Jon P. Camden.

Chris B. Milojevich, Daniel W. Silverstein, Lasse Jensen, and Jon P. Camden. **Surface-Enhanced Hyper-Raman Scattering Elucidates the Two-Photon Absorption Spectrum of Rhodamine 6G.** The Journal of Physical Chemistry C (2013), 117 (6), 3046-3054.

The article is represented in the form which it was published, with the exception that the following JPC required sections have been removed: Acknowledgements, Author Information, and Notes. The dissertation author conducted all of the experiments indicated in the paper, designed each of the figures, and wrote the bulk of the paper. The calculations and theoretical methods indicated in the paper were conducted and written by DW Silverstein and L Jensen. All authors contributed equally and approved the final document.

Abstract

The surface-enhanced hyper-Raman (SEHRS) spectra of Rhodamine 6G (R6G) are measured for two different excitation energies, ~25000 cm^{-1} (~810 nm) and ~19000 cm^{-1} (1030 nm). The collected spectra are compared to time-dependent density functional theory simulations of the resonance hyper-Raman spectra for the same excitation energies. The analysis of molecular orbital changes in these nonlinear transitions

elucidates the mechanism of vibronic enhancement. This analysis is used to elucidate features in the two-photon absorption spectra of R6G.

Introduction

The last decade has seen an exponential increase in the exploration and utilization of multi-photon processes.[1] Two-photon transitions, for example, play essential roles in energy up-conversion,[2, 3] all-optical switching,[4, 5] optical data storage,[6, 7] 3D lithography,[8, 9] and biological imaging.[10- 14] The recent availability of "turn-key" mode-locked lasers further promises intense future interest in nonlinear spectroscopy. The use of two-photon excited fluorescence, for example, has become routine in microscopy imaging studies, yet very little is known about the two-photon properties of even routine nonlinear chromophores, such as Rhodamine 6G.

Often, in engineering molecules suitable for two-photon fluorescence, the two-photon absorption (TPA) spectrum is used as an indicator of the relative "strength" of the two-photon properties of a molecule. Analyzing the TPA spectrum, however, is often difficult and it is rarely possible to make definitive assignments to the various absorption features by relying only on TPA experiments. The inclusion of theoretical calculations can significantly improve the situation; however, accurate calculations of nonlinear molecular properties remain a formidable challenge. Given the lack of discrete information in the two-photon absorption spectra and calculations, it is necessary to use other two-photon processes, such as hyper-Raman spectroscopy (HRS), to aid in the interpretation of the spectra.

Hyper-Raman scattering is a type of nonlinear spontaneous light scattering, which gives rise to frequencies of $2\omega_E \pm \omega_v$, where ω_E is the incident frequency and ω_v is a molecular vibration frequency. The hyper-Raman effect was first reported in 1965 by Terhune, Savage, and Maker[15] and recent progress in the application of hyper-Raman spectroscopy was recently reviewed by Myers Kelley.[16] Although multiphoton processes, such as hyper-Raman scattering, afford advantages such as higher selectivity, decreased risk of photo-damage to the sample, and higher penetration depth,[13, 17] the detected intensities of the processes are significantly lower. For the same laser intensity and nonresonant conditions, it has been estimated that hyper-Raman scattering intensities are 5 to 7 orders of magnitude weaker than Raman scattering intensities.[18] For many molecules it is, therefore, beneficial to make use of surface[19-28] and resonance[29-35] enhancements to detect hyper-Raman scattering.

In previous works, we utilized both resonance and surface enhancements to show non-Condon scattering can dominate a resonant hyper-Raman (RHR) spectrum and this information can be used to assign features in the two-photon absorption spectrum of R6G.[36, 37] After a reviewing prior RHR studies of Rhodamine 6G and the theortical framework for RHR calculations, we make a detailed comparison between theoretical simulations and experimental measurements of RHR spectra of R6G. This combined approach provides a detailed interpretation of the seemingly contradictory SERS and SEHRS spectra of Rhodamine 6G. In the process, the mechanism of the one- and two-photon electronic transitions in R6G around 19000 wavenumbers emerges; thus

demonstrating the power of resonance hyper-Raman studies to elucidate the features in two-photon absorption spectra.

Nonlinear Spectroscopy of Rhodamine 6G

Rhodamine, a xanthene derivative, is one of the most popular molecules to modify as a two-photon dye[38, 39]. Rhodamine dyes or derivatives have recently been used as two-photon fluorescence probes for mercury ions in live cells,[11] as multi-photon probes for exploring diffusion in vivo skin samples,[12] and as benchmark molecules in two-photon excitation systems[13]. The first SEHRS of R6G, reported in 1982 by Baranov and Bobovich[19] dates from the earliest days of surface-enhanced vibrational spectroscopy. Their pioneering study compared SEHRS and SERS of R6G at excitation wavelengths of 1064 and 532 nm, respectively, and found dramatic differences between the two. Figure 14 displays SEHRS spectra at 1028 nm and SERS spectra at 514 nm for R6G, illustrating these differences. Even though both spectra are measured at equivalent energies for the respective processes, the two spectra share very few common peaks and the peak intensities are drastically different. Even 30 years this observation, the origin of these differences has not been satisfactorily explained, despite numerous studies of the two-photon properties of R6G. [19, 31, 38, 40, 41]

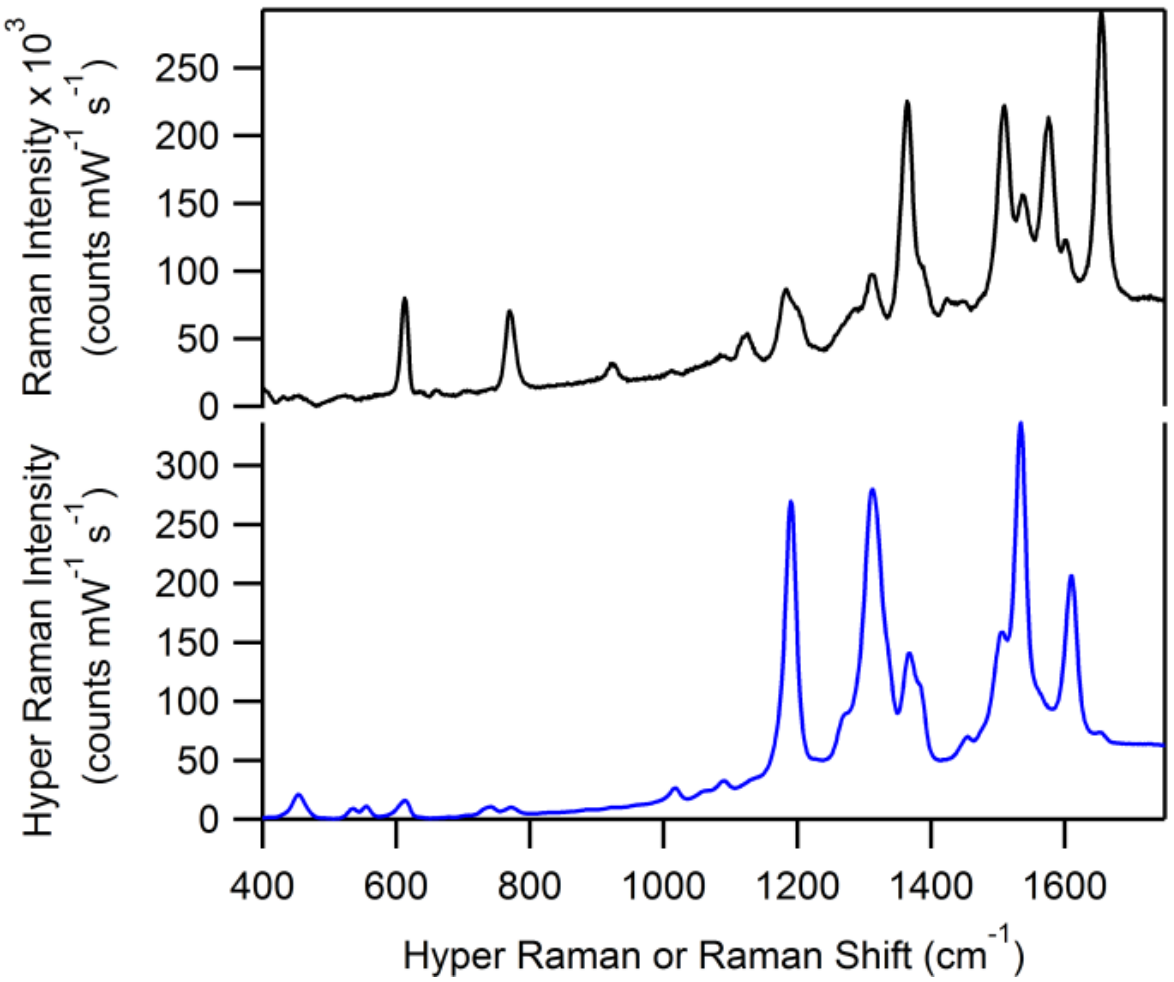


Figure 14. A comparison of SERS (top, P = 300 μW, t_{acq} = 5 s) and SEHRS (bottom, P = 6 mW, t_{acq} = 120 s) of R6G (10^{-6} M) on aggregated Ag colloids taken at excitations of 514 and 1028 nm, respectively.

In Figure 15, the one- and two-photon[42] absorption spectra of R6G between 18000 and 27000 wavenumbers are presented. In the spectra, a peak is observed in the 19000 wavenumber region of the one photon absorbance, which corresponds to a much smaller peak in the two photon absorption spectrum. This absorption in R6G is labeled as S_1 and is the first excited singlet state. The existence of both a one- and two-photon absorption suggests that the S_1 transition is both one- and two-photon allowed and therefore the $S_1 \leftarrow S_0$ electronic transition is not governed by parity of the states involved. A lack of symmetry elements for S_1 and S_0, implies that the resonance enhanced SERS and SEHRS spectra should be identical; however, this is clearly not supported by the experimental RHR spectra. Initial theories[19, 31, 40] suggested that the spectral differences resulted from a local symmetry breaking in the molecule: the molecule becomes distorted on the surface of the metal or by anions in solution, and this allows transitions of the molecule which would be otherwise forbideen. The simple picture of symmetry "allowed" or "forbidden" transitions, however, does not sufficiently explain the nonlinear scattering spectrum. In particular, the S_2 state at approximately 25000 wavenumbers appears to be two-photon allowed, and one-photon forbidden; a contradiction that should not exist if the molecule has no symmetry. In fact, Rhodamine is a relatively weak two-photon scatterer at 19000 wavenumbers, compared to other nonlinear chromophores in the same region.[42] Understanding the mechanism of the two-photon accessible electronic transitions in such a complex molecule is almost impossible if one

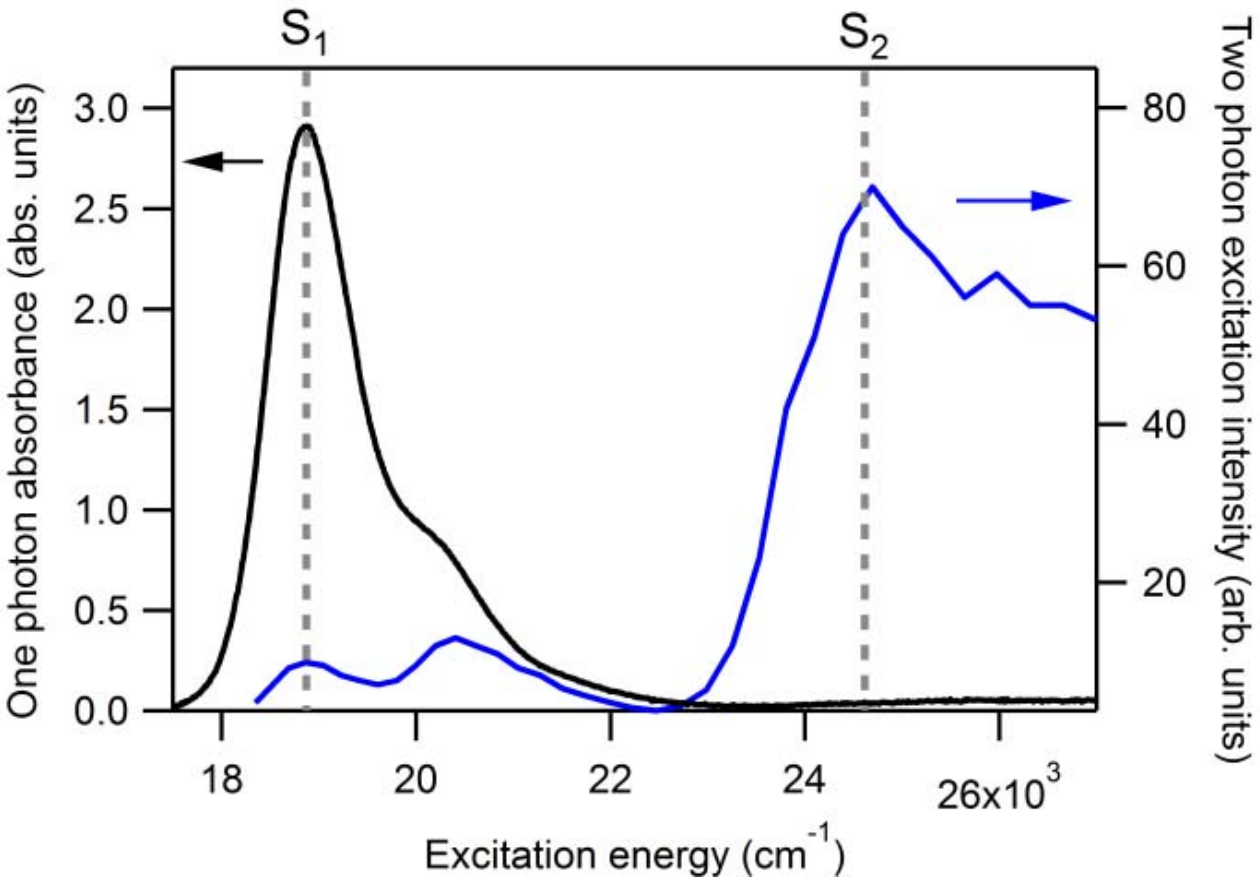


Figure 15. The one-photon absorbance and two-photon excitation spectra[42] are shown for Rhodamine 6G. Also indicated are two transitions within the molecule: S_1, which is one and two-photon accessible, and S_2, which is only two-photon accessib

utilizes only two-photon fluorescence or hyper-Raman spectroscopy, however, understanding can be achieved by examining both spectroscopies.

In the past, our group utilized both theoretical simulations and hyper-Raman experiments to show that RHR calculations can contribute greatly to understanding the transitions between electronic states which are probed by nonlinear spectroscopy.[37] Recently, we showed that vibronic coupling enables the one-photon allowed but two-photon forbidden state to contribute significantly to both hyper-Raman scattering and two-photon fluorescence in this region.[36] However, the the physical mechanism which facilitates the vibrational coupling in RHR remains unexplored, and constitutes the subject of this work. Understanding of such mechanisms should also shed light on the nonlinear properties of the molecule, such as its two-photon absorption profile.

Resonance Hyper-Raman Calculations

Simulations of RHR scattering require calculation of the resonant first hyperpolarizability, which is a formidable task, and one which is more computationally demanding than the calculations of the resonant polarizability for resonance Raman (RR) scattering. This challenge can be reduced by employing the vibronic theory of RHR scattering developed by Ziegler *et al.*[43] in combination with the time-dependent wavepacket approach.[44, 45, 46, 47, 48] The vibronic theory for RHR involves writing the hyperpolarizability of the molecule as a sum of terms: $\beta = A + B + C + \ldots$, where A is the Franck-Condon (FC) term, B is the first Herzberg-Teller (HT) term, C is the second HT term, etc. Several studies have

demonstrated the utility of the vibronic theory for analyzing experimental observations and the feasibility of RHR simulations for predicting spectra in comparison to available experimental data.[26, 34, 35, 49, 50] Furthermore, it has been found that RHR scattering is sensitive to non-Condon effects, possibly more so than resonance Raman scattering.[36, 51] This feature is related to the selection rules of hyper-Raman scattering, which are complementary to Raman and IR, allowing forbidden IR and Raman-active vibrations to be hyper-Raman active.

Figure 16 demonstrates three important cases to consider in the discussion of resonance hyper-Raman spectra. The following discussion assumes an electronic transition $S_k \leftarrow S_0$, where S_0 is the ground electronic state and S_k refers to the kth singlet excited electronic state. In A-term scattering the transition is allowed via both one-photon and two-photon absorption. Therefore, both the two-photon transition dipole moment (S^{k0}) and the one-photon transition dipole moment (μ^{0k}) have non-zero values. In this case, the resonance hyper-Raman scattering is calculated using the FC overlap between the initial and final vibrational states of the molecule and, just as in resonance Raman, these overlap terms are called “A-term” contributions to the resonance hyper-Raman spectrum or A-term scattering, for short.[52, 53, 54] The notation S^{k0} refers to the amplitude of the two-photon excited transition $S_k \leftarrow S_0$, and should not be confused with the labeling of the singlet electronic states (e.g. S_0, S_1, S_k, …).

In the other two cases, the transition is allowed in either the two-photon absorption or the one-photon absorption, but is forbidden or weakly allowed, in

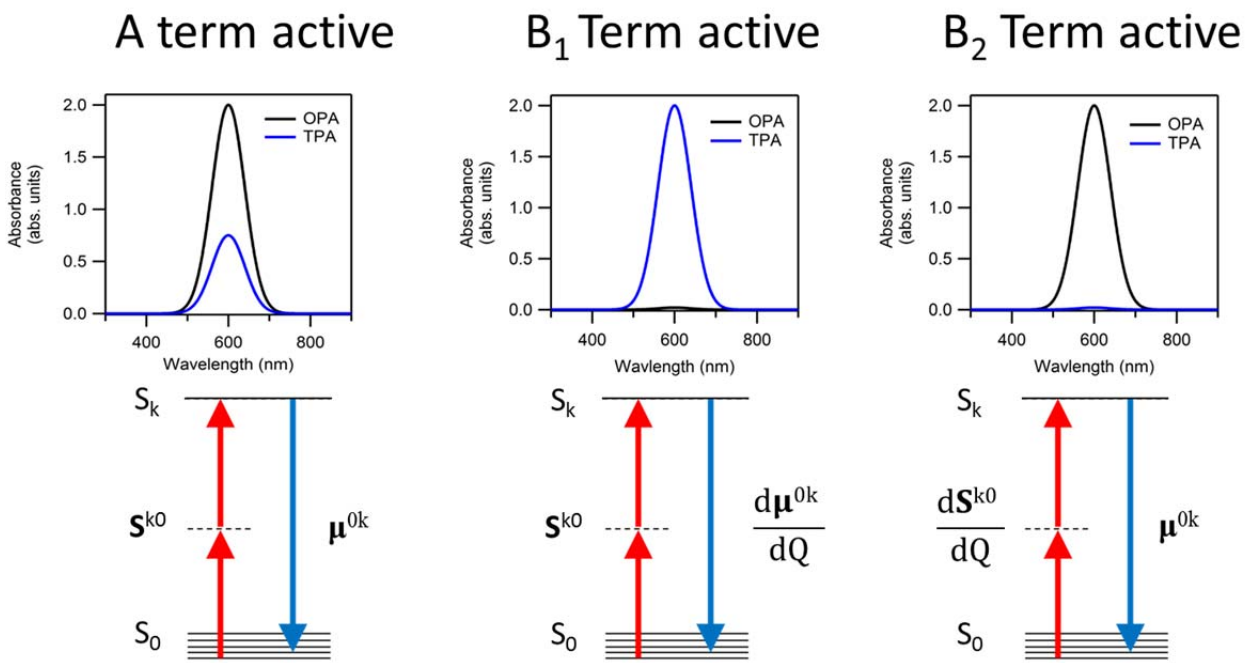


Figure 16. Terms included in the calculation of resonance hyper-Raman spectra. In a both one- and two- photon allowed transition $S_k \leftarrow S_0$, both the two-photon transition dipole (S^{k0}) and one-photon transition dipole (μ^{0k}) are non-zero. However, in cases where the one-photon transition is forbidden/weakly allowed (μ^{0k} is zero or nearly zero) or where the two-photon transition is forbidden/weakly allowed (when S^{k0} is zero or nearly zero), then vibronic coupling may produce non-zero terms ($d\mu^{0k}/dQ \frac{d\mu^{0k}}{dQ}$ and dS^{k0}/dQ, respectively) that contribute to the resonant hyper-Raman calculation at these wavelengths.

the other absorption. For these, at least one of the transition dipole moments (μ^{0k} or S^{k0}) is zero or very small, which leads to weaker resonance hyper-Raman intensity via A-term scattering for that transition. In the well-known Condon approximation, it is usually assumed that μ^{0k} or S^{k0} do not depend strongly on the nuclear coordinates (Q). Molecular vibrations, however, can couple together nearby electronic states via the derivative of the one-photon transition dipole moment ($d\mu^{0k}/dQ$) or of the two-photon transition dipole moment (dS^{k0}/dQ). These terms provide an addition mechanism for the enhancement of the resonance hyper-Raman cross section. It is important to realize that although the two-photon transition dipole moments are calculated directly using quadratic response theory is formally contains a sum over all intermediate states. This is valid as long as the incident light is not resonant with any intermediate states. The direct calculation of the two-photon transition moments is computational advantageous since it avoids the explicit sum, however, it also means that individual contributions from intermediate states cannot be identified. The couplings terms can be calculated by the HT approximation, and as in resonance Raman, these terms are referred to as “B-term” contributions. In RHR they are divided into two types: B_1, where the two-photon transition is allowed, and the one-photon transition is vibronically coupled; and B_2, where the one-photon transition is allowed, and the two-photon transition is vibronically coupled.

Experimental Methods

Experimental Set-up

The experimental set-up, similar to ones used in previous experiments[37], is shown in Figure 17. In detail, the pump laser used is capable of 15 W of continuous wave 532 nm radiation (Millenia Pro, Spectra-Physics). The oscillator is a Ti: sapphire (Tsunami, Spectra-Physics), which is equipped with broadband optics to allow the ~5 ps pulse to be tuned to a selected wavelength between 690 and 1080 nm. The fundamental from the Ti: sapphire is split, using a combination half-wave plate (Thor Labs) and Glan polarizer (Thor Labs). The horizontal polarization is used to irradiate the sample, while the vertical polarization is frequency doubled via a second harmonic generator (SHG, Model 3890, Spectra-Physics). The excitation beam is directed into the back port of an inverted microscope (Ti-U, Nikon), through a 20x, NA = 0.5, objective (Nikon) which is focused on the sample. A 690 nm short pass filter (Semrock) is used to reduce the intensity of the laser line before it is reflected to the spectrometer (Acton, Princeton Instruments). The detector is a back-illuminated CCD camera (Spec-10, Princeton Instruments) which is operated using either the commercially available Winspec (Princeton Instruments) or a homebuilt LabView program.

SERS/SEHRS sample preparation and use

Collodial silver nanoparticles were synthesized using the Lee and Meisel method.[55] Specifically, 200 mL of 2×10^{-3} M silver nitrate (Sigma Aldrich) is

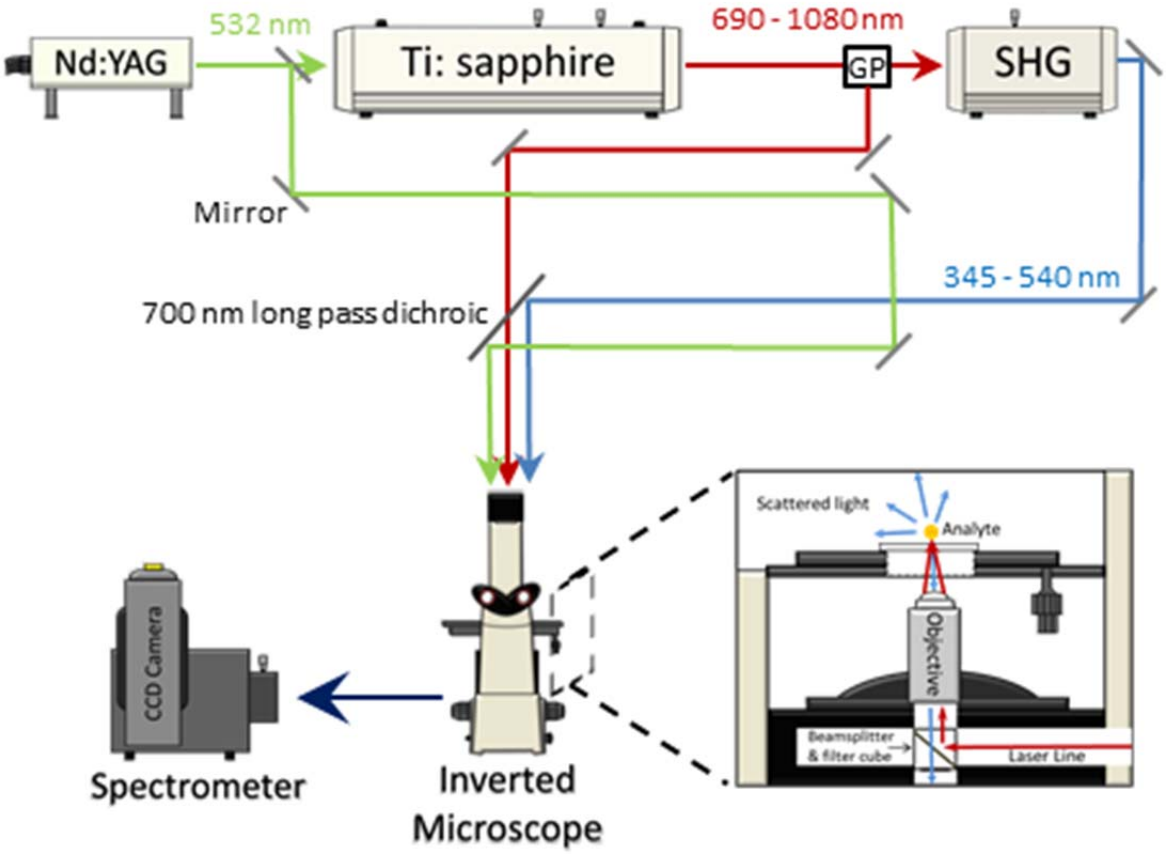


Figure 17. Experimental set-up for surface-enhanced and bulk Raman and hyper-Raman experiments. An Nd:YAG pumped Ti:Sapphire output is split using a half-wave plate and Glan-Polarizer (labeled GP on diagram). The vertical polarization is sent to a second harmonic generator (SHG) and the horizontal polarization is converted to vertical before entering the scope (using a periscope – not pictured).

brought to a boil. Then, 50 milligrams of sodium citrate monohydrate (Sigma Aldrich) dissolved in a small amount (~5 mL) of water is added. After approximately 30 minutes, the volume of the solution is less than 150 mL, and has turned a light green in color. The solution is then removed from the heat source, and allowed to cool. This produces mostly spherical nanoparticles around 30 nm in diameter. 30 mL of this solution is then mixed with 1 mL of 10^{-5} M R6G (Acros). The nanoparticles almost immediately begin to crash out, as the solution turns dark. Sodium bromide (Sigma Aldrich) is then added to this sample to produce a final concentration of 10^{-2} M bromide ions. The colloids are allowed to aggregate into clusters which average approximately 1-2 microns in size. For hyper-Raman measurements, approximately 6 mW of laser power is focused on one of these aggregates. Rastering the sample prevents the ablation of the nanoparticle aggregates, due to the high laser power used. Since the hyper Rayleigh scattering from the sample is approximately the same order of magnitude as the hyper-Raman, no filter was needed to limit its intensity. In Raman measurements, less than 1 mW of laser power is focused on an aggregate. Since the Rayleigh line is much more intense than the Raman lines, a filter must be used to limit its intensity.

Theoretical Methods

Geometry optimization and normal mode calculations were performed in NWChem using B3LYP/6-311G*.[56] These calculations yield both vibrations of the molecule and IR intensities. For all simulations, the normal modes were

scaled by a constant factor of 0.98. Dimensionless displacements (Δ), transition dipole moment derivatives (dμ/dQ), and two-photon transition moment derivatives (dS/dQ) were evaluated using finite differentiation of properties calculated with the linear and quadratic response modules in Dalton 2.0 with B3LYP/6-311G*.[57] Empirical solvent shifts on the order of 0.20 to 0.56 eV were applied to each excitation to facilitate comparison with experimental data. A detailed description of the simulation procedure can be found in previous publications. [58, 59] However, a simplified physical description of the calculated scattering "terms" is included here.

The simulations of vibronic coupling are based on the time-dependent wavepacket approach pioneered by Heller *et al*.[14] Focusing on the expression for RHR (e.g. $\boldsymbol{I^{RHR}} \propto |\boldsymbol{\beta}|^{\mathbf{2}})\mathrm{I}^{\mathrm{RHR}} \propto |\beta|^{2})$, the sum-over-states expression for the molecular first hyperpolarizability is written using the Born-Oppenheimer approximation and expressed in the time-domain by using a Fourier transform. The result is then simplified by employing the time-propagator for the kth excited state and closure over the corresponding intermediate vibrational states. Vibrational overlaps in this method are evaluated using the independent-mode, displaced harmonic oscillator model. The one-photon transition dipole moment (μ^{0k}) and two-photon transition dipole moment (S^{k0}) can then be expanded in a series with respect to the normal modes:

$$\mu^{0k} = \left(\mu^{0k}\right)^{eq} + \sum_a \frac{\partial \mu^{0k}}{\partial Q_a} Q_a + \ldots \mu^{0\mathrm{k}} = (\mu^{0\mathrm{k}})^{\mathrm{eq}} + \sum_{\mathrm{a}} \frac{\partial \mu^{0\mathrm{k}}}{\partial \mathrm{Q_a}} \mathrm{Q_a} + \cdots$$

(1)

and,

$$S^{k0} = \left(S^{k0}\right)^{eq} + \sum_b \frac{\partial S^{k0}}{\partial Q_b} Q_b + \ldots$$

(2)

where the superscript "eq" refers to a quantity evaluated at the ground state equilibrium geometry. Based on the series expansions, we can write the first hyperpolarizability as a series: $\beta = A + B_1 + B_2 + \ldots$ where the A term is the FC term and B_1/B_2 are the first HT terms. The final expressions are for A, B_1, and B_2 are written as a product between the transition dipole moments connecting the ground state to the kth excited state and a lineshape function containing vibronic information, i.e.:

$$A = \sum_k \left(\mu^{0k}\right)^{eq} \left(S^{k0}\right)^{eq} \cdot L[E^{k0}, \Delta_{\mathrm{v}}^{k0}, \omega_{\mathrm{v}}, \omega_E, g_k(t)] \tag{3}$$

$$B_1 = \sum_k \sum_a \frac{\partial \mu^{0k}}{\partial Q_a} \left(S^{k0}\right)^{eq} \cdot M_a[E^{k0}, \Delta_{\mathrm{v}}^{k0}, \omega_{\mathrm{v}}, \omega_E, g_k(t)] \tag{4}$$

$$B_2 = \sum_k \sum_b \left(\mu^{0k}\right)^{eq} \frac{\partial S^{k0}}{\partial Q_b} \cdot N_b[E^{k0}, \Delta_{\mathrm{v}}^{k0}, \omega_{\mathrm{v}}, \omega_E, g_k(t)] \tag{5}$$

Where E^{k0} is the electronic excitation energy, $\Delta_{\mathrm{v}}^{k0}\Delta_{\mathrm{v}}^{k0}$ is the vibronic coupling constant for the normal mode with frequency ω_{v}, ω_E is the incident frequency, and $g_k(t)$ is a function defining the homogeneous and inhomogeneous

broadening for the kth excited state. Specific forms of the lineshape functions L, M_a, and N_b can be found in prior publications.[58, 59]

The vibronic model described above relies on the harmonic oscillator model to evaluate overlaps between vibrational states. This means that normal modes sensitive to anharmonic effects are poorly described by the present model. Also, Duschinski rotations are neglected, i.e. ground and excite states are assumed to have identical vibrational frequencies. The determination of the vibronic coupling constants is sensitive to the description of the electronic structure in the ground and excited states in addition to the molecular geometry. Therefore, the choice of the exchange-correlation functional from density functional theory is paramount to describing the potential energy surface, excitation energies, and transition moments accurately. Furthermore, it is required that the electronic states are well separated to ensure that the numerical evaluation of the derivatives required to obtain vibronic coupling constants and the B_1 and B_2 terms remain valid. For R6G, the S_1 and S_2 states are separated by approximately 0.35 eV for the functional chosen here, allowing for the derivatives to be evaluated accurately.

Results

Vibronic Coupling in Resonance Hyper-Raman Spectra

A comparison of the experimentally measured and theoretically simulated hyper-Raman spectrum on resonance with the $S_1 \leftarrow S_0$ transition (19000 cm^{-1}) is

displayed in Figure 18. We previously showed that inclusion of the B-type scattering terms is required to achieve agreement between experiment and theory in this region.[36] Here we expand that observation to explore the relative contributions of the A, B_1, and B_2 terms. At this energy (19000 cm^{-1}, 1030 nm) a small contribution from A-term scattering is visible; however, the majority of the spectrum results from B_2 term. While $S_1 \leftarrow S_0$ is a strong one-photon transition, it has a small two-photon dipole transition moment (S^{10}); therefore, vibrations which modify the transition moment (dS^{10} / dQ) are featured prominately in the resonance hyper-Raman spectrum. Further, Figure 5 illustrates that the spectrum at this excitation energy is almost entirely dominated by the B_2 term.

It is interesting to contrast this results in Figure 18 ($S_1 \leftarrow S_0$) with spectra obtained on resonance with the $S_2 \leftarrow S_0$ (24000 cm^{-1}, 820 nm), which is given in Figure 19. No contribution from the A term contribution is evident, as the $S_2 \leftarrow S_0$ transition is only two-photon allowed (see Figure 15). Instead, the spectrum is dominated by B_1-term scattering. The one-photon transition dipole moment (μ^{02}) is close to zero, and the vibrationally coupled dipole moment ($d\mu^{02}$ / dQ) is non-zero. Interestingly, a significant portion of the hyper-Raman spectrum on resonance with $S_2 \leftarrow S_0$ can be attributed to B_2 scattering, even though the transition is two-photon allowed and one would expect the two-photon transition dipole moment (S^{20}) to be greater than its vibrationally coupled

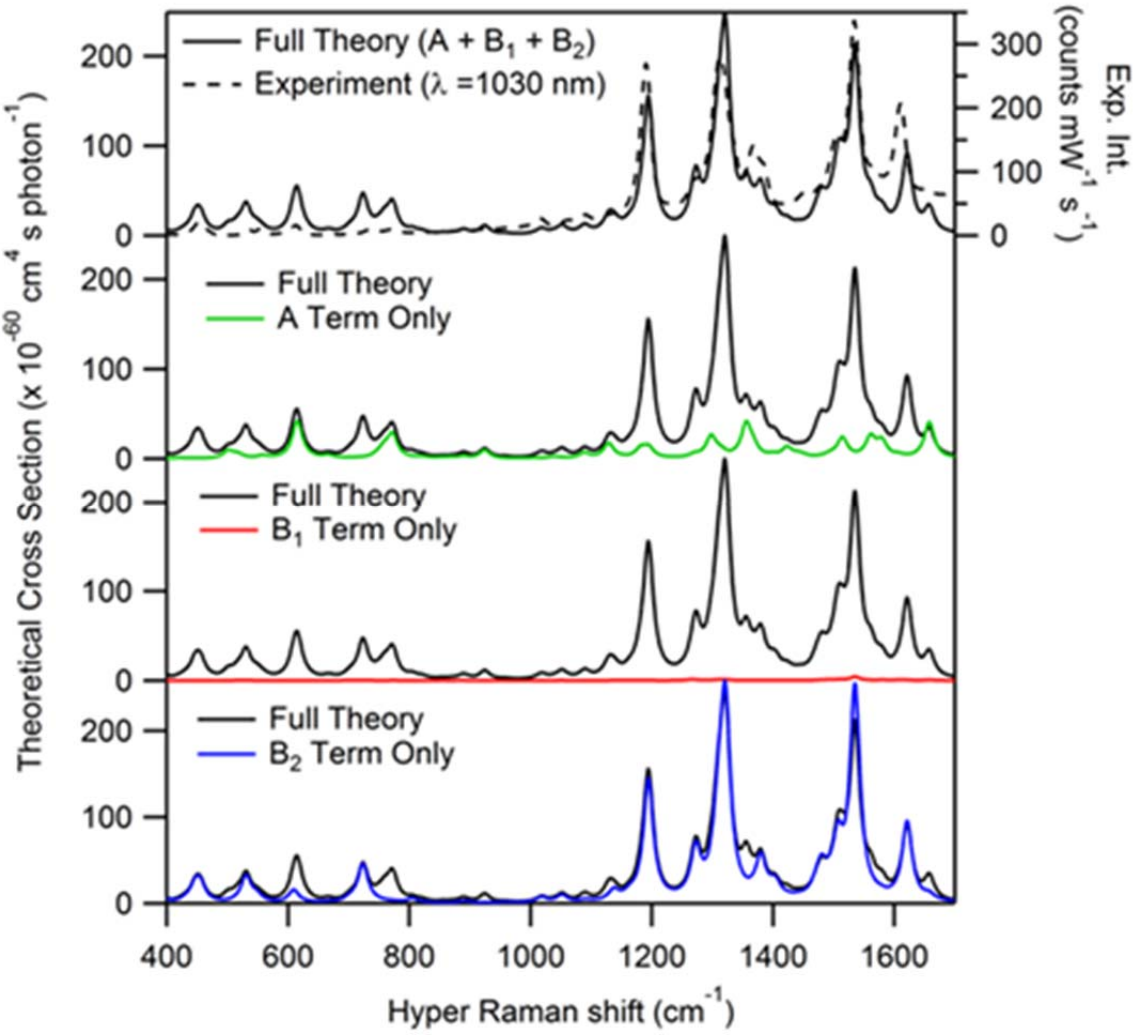


Figure 18. Comparison of experimental and calculated resonance hyper-Raman spectra at an excitation energy of 19000 cm^{-1} (1030 nm). The contributions to the simulated spectra from the individual resonance hyper-Raman terms are also presented: A term (FC), B_1 term (HT), and B_2-term (HT). At this energy the RHR scattering is dominated by B_1 activity.

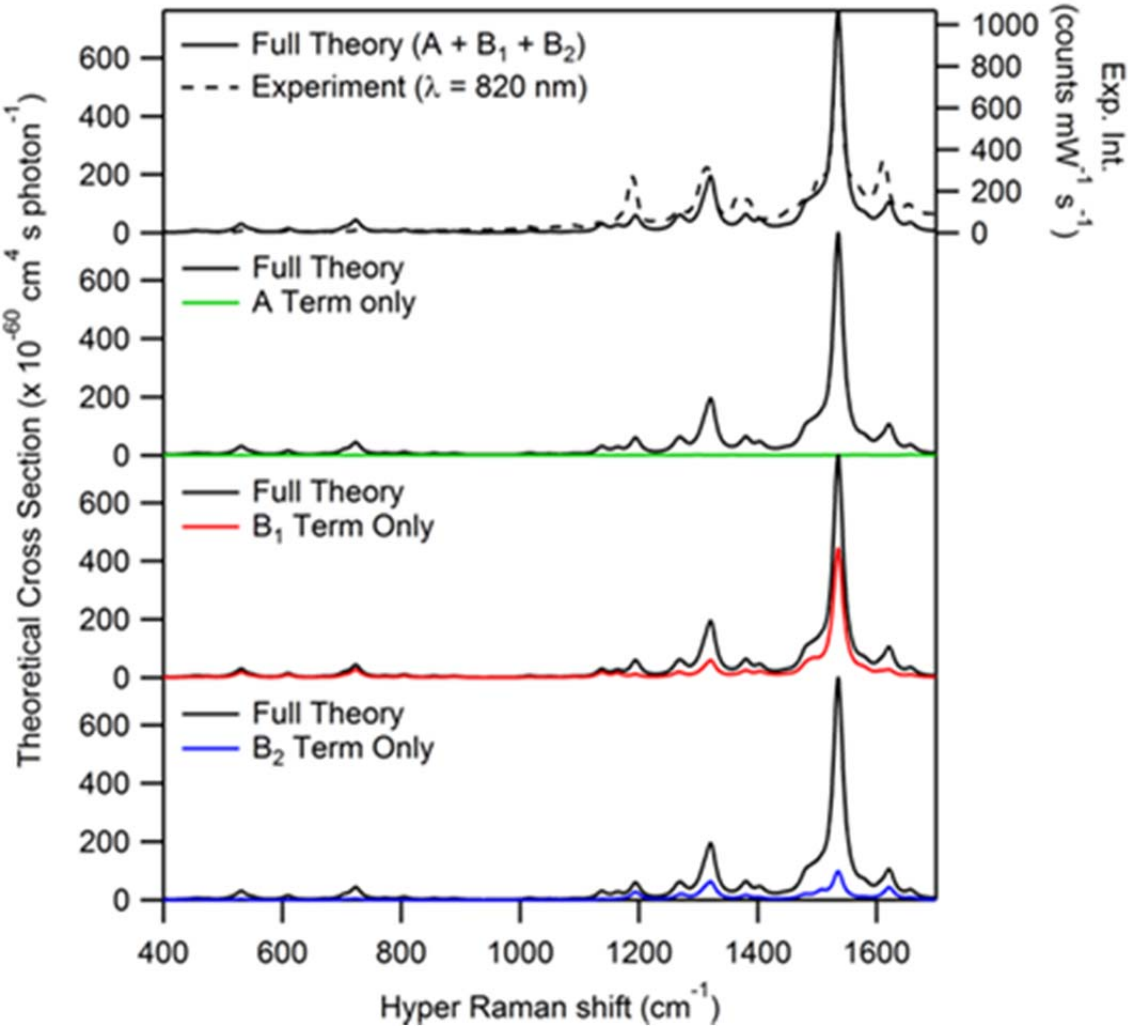


Figure 19. Comparison of experimental and calculated resonance hyper-Raman spectra at an excitation energy of of 24000 cm^{-1} (810 nm). The contributions to the simulated spectra from the individual resonance hyper-Raman terms are also presented: A term (FC), B_1 term (HT), and B_2-term (HT). At this energy the RHR scattering is dominated by B_1 activity.

derivative (dS^{20} / dQ). Therefore, we must conclude that scattering at this wavelength involves significant interference between the $S_2 \leftarrow S_0$ and the $S_1 \leftarrow S_0$ transitions, even though their absorption bands do not overlap. Further theoretical and experiments investigations may reveal this to be a more common feature of RHR scattering than previously anticipated.

For $S_1 \leftarrow S_0$ and $S_2 \leftarrow S_0$ transitions in R6G, the magnitude of the B term contributions to RHR scattering is unusual based on comparisons to other molecules that are A term scatterers in RR and RHR. In RR scattering, B terms (governed by μ^{0k} and $d\mu^{k0}/dQ$) are expected to have low intensity because the transition must be weakly allowed. RHR scattering, in contrast, has B terms governed by the two mechanisms described in Figure 16 (i.e. the transition is one-photon forbidden/two-photon allowed for B_1 term scattering or one-photon allowed/two-photon forbidden for B_2 term scattering). The structure of R6G possesses nearly C_s symmetry, with a mirror plane containing the carboxyphenyl ring (see Figure 20). This causes the one- and two-photon transitions to be mutually exclusive because R6G is almost centrosymmetric. Therefore, the intense B term scattering on resonance with the $S_1 \leftarrow S_0$ and $S_2 \leftarrow S_0$ transition is justified since the one- and two-photon transitions cannot simultaneously be strong.

One- and Two-photon Absorption Spectra: Theory and Experiment Comparison

Figure 20 displays the transitions and associated molecular orbitals for Rhodamine 6G in the 18000 to 27000 cm^{-1} energy range (center panel). Here we designate the highest occupied molecular orbital (HOMO) to lowest unoccupied molecular orbital (LUMO) ($S_1 \leftarrow S_0$) and HOMO-1 to LUMO ($S_2 \leftarrow S_0$) transitions as S_1 and S_2. Comparison of the experimental one-photon absorption and two-photon absorption[32, 59] with simulated spectra are shown in the left and right panels, respectively. The simulated results incorporate the empirical shifts described in the Theoretical Methods, and spectra obtained with and without vibronic effects are presented. When vibronic effects are included, we further compare spectra obtained with only FC couplings (green line) and those obtained with a sum of FC and HT terms (red line).

The molecular orbitals (Figure 20) illustrate that R6G has local symmetry associated with the S_1 and S_2 electronic states, due to the localization of the orbitals in the xanthene ring. Assuming C_s symmetry, the HOMO is anti-symmetric in the σ_v plane, while the LUMO and HOMO-1 are symmetric in the same plane. An excitation from HOMO to LUMO must be accompanied by a change in symmetry, and therefore will be one-photon allowed but *not* two-photon allowed. This transition ($S_1 \leftarrow S_0$) occurs at 19000 cm^{-1} (~530 nm via one photon transition). The transition from HOMO-1 to LUMO is not accompanied by a change in symmetry, and therefore is expected to be two-photon allowed but

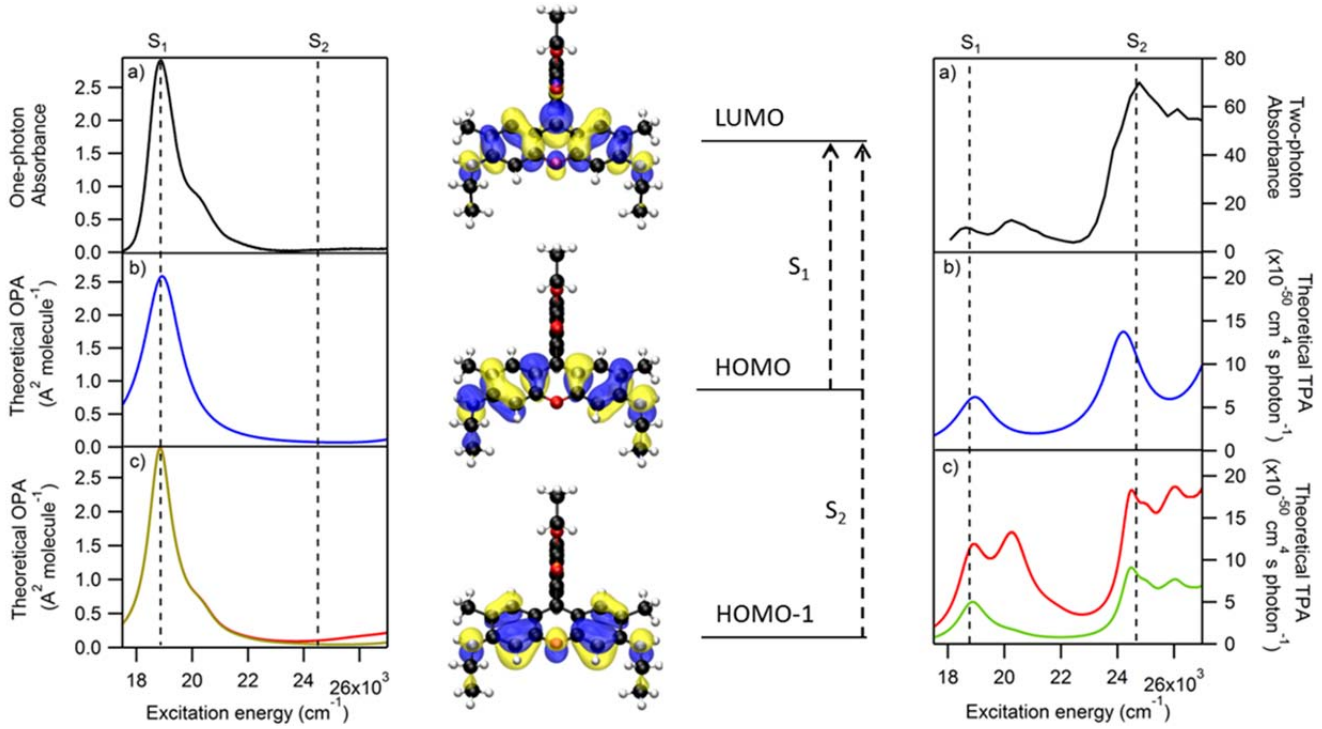


Figure 20. Comparison of one-photon absorption spectra (left) to the two-photon absorption spectra[32] (right) of Rhodamine 6G and the electronic transitions excited in the molecular orbitals (middle). The absorption spectra are broken into three parts: a) the experimental absorption spectrum, b) the theory simulated spectrum without vibronic coupling (Lorentzian broadened with 0.10 eV full-width at half maximum), and c) the theory simulated absorption spectra, calculated with FC vibronic coupling (orange) and with FC and HT vibronic coupling (red) spectra.

not one-photon allowed. This transition, which is assigned to S_2, occurs at 24000 cm^{-1} (~405 nm). No other transitions are identified in the 18000 cm^{-1} - 23000 cm^{-1} region in either experiment or theory.

The one-photon absorption spectra (Figure 20, left panel) follow the expectation established by the molecular orbitals: the $S_1 \leftarrow S_0$ transition is dominant and the $S_2 \leftarrow S_0$ transition is nearly zero. The simulated spectra are in good agreement with experiment and the shoulder that occurs to the red of the main $S_1 \leftarrow S_0$ transition (~20000 cm^{-1}) does not appear in the purely electronic transition spectrum. When FC vibronic coupling is included in the absorption simulations, however, the shoulder appears in the spectrum. This shows that there is a non-zero component contribution from the FC term to the one-photon absorption spectrum. This agrees with previous simulations of one-photon absorption for the $S_1 \leftarrow S_0$ transition of R6G.[60] When HT coupling is included in the one-photon absorption calculations, very little change is observed, since the HT term contribution to the one-photon absorption spectrum is very weak.

The two-photon absorbance spectra (Figure 20, right panel) deviate from the spectrum expected based purely on the symmetry of the molecular orbitals. While the $S_2 \leftarrow S_0$ transition shows a strong absorption band, as expected, $S_1 \leftarrow S_0$ also appears in the experimental and theoretical spectra. The most likely reason for this weakly allowed transition is that, in both HOMO and LUMO, there are portions of the electronic structure that extend into the phenyl ring. These components have a symmetric overlap that makes the S_1 transition in the two-

photon absorption weakly allowed. In the FC vibronic coupling spectra, a shoulder, centered around 26000 cm^{-1}, appears for the S_2 state, which mimics the shoulder in the experimental spectrum. However, the shoulder that appears in the S_1 spectrum, centered around 20000 cm^{-1}, only appears when the HT vibronic coupling is included in the simulations. It is evident from this comparison that the full understanding of the two-photon absorption spectrum can only be achieved through use of HT vibronic coupling terms. We have further confidence in this assignment from the strong B-term contribution to the RHR scattering in this region. Improvement of the intensities of the S_1 and S_2 may require including a solvent model in the calculations of excited state properties[60, 61] or changing the exchange-correlation functional used.

Origin of the non-Condon Scattering

Using a molecular orbital approach it is further possible to understand why only select vibrational modes of the R6G molecule experience a strong hyper-Raman enhancement. The diagrams in Figure 21 and Figure 22 indicate the orbitals involved in the $S_1 \leftarrow S_0$ and $S_2 \leftarrow S_0$ transitions respectively and, additionally, illustrate the changes in the orbitals induced by vibration along the 1535 cm^{-1} coordinate. This mode was selected as it shows the greatest intensity in the $S_1 \leftarrow S_0$ and $S_2 \leftarrow S_0$ resonance spectra. The difference orbitals are generated by subtraction of the absolute value of the original molecular orbital from the absolute value of the perturbed molecular orbital. The perturbed orbital is calculated after a 1% displacement along the vibrational coordinate. The green

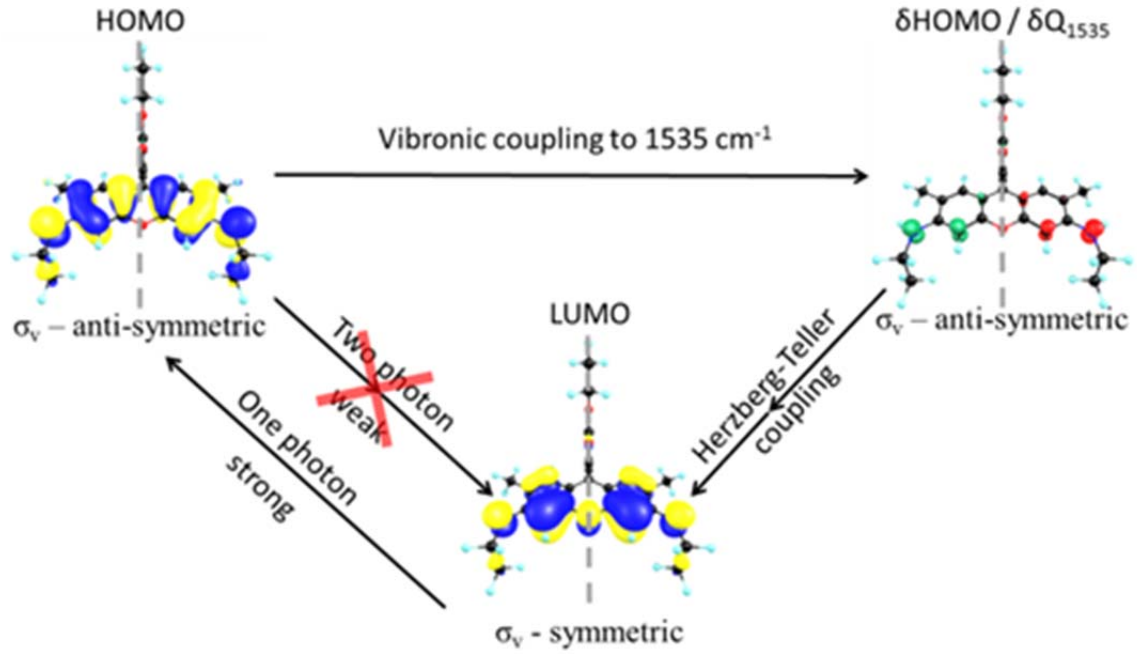


Figure 21. Molecular orbitals involved in the $S_1 \leftarrow S_0$ transition. The transition from HOMO (upper left) to LUMO (lower) is symmetry forbidden for a two-photon transition, as it involves a transition from an asymmetric orbital to a symmetric orbital. However, vibronic coupling of the 1535 cm^{-1} vibration to the HOMO yields asymmetric changes (upper right - red indicates a negative change, green a positive change) in the HOMO which allows a two-photon transition to the symmetric LUMO.

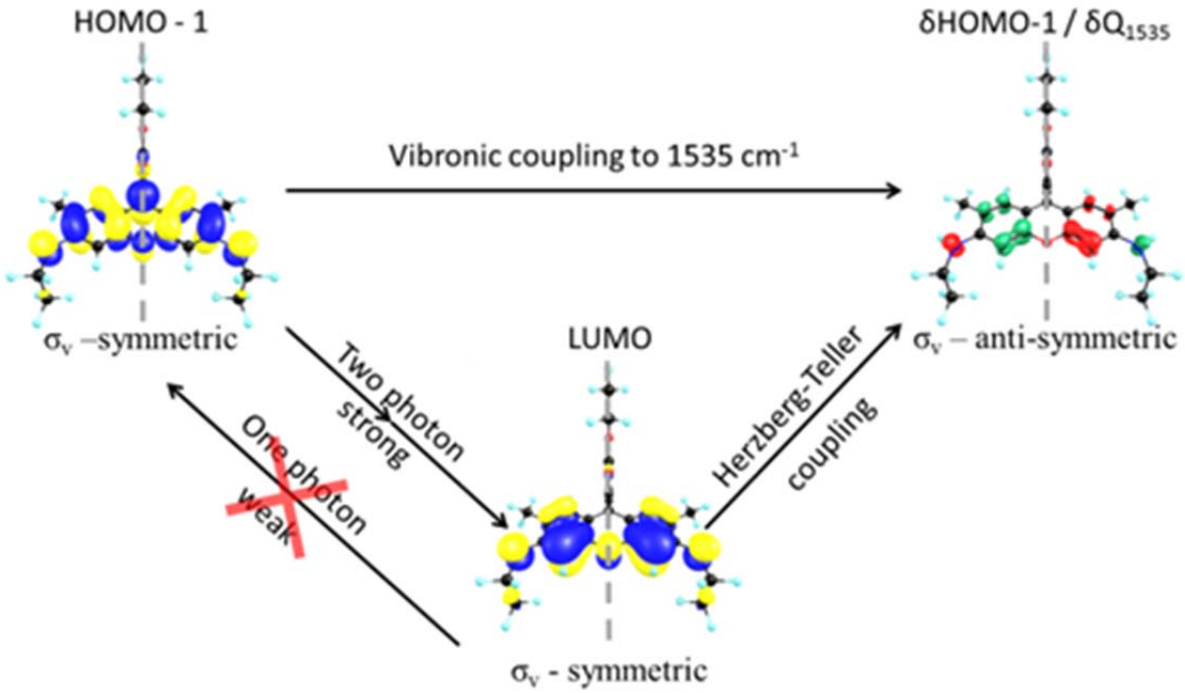


Figure 22. Molecular orbitals involved in the $S_2 \leftarrow S_0$ transition. The transition from LUMO (lower) to HOMO-1 (upper left) is symmetry forbidden for a one-photon transition, as it involves a transition from a symmetric orbital to a symmetric orbital. However, vibronic coupling to the 1535 cm^{-1} vibration yields asymmetric changes (upper right – red indicates a negative change, green a positive change) in the HOMO-1 which allows a two-photon transition to the symmetric LUMO.

areas represent where the orbital increased, and the red represent areas where the orbital decreased.

As can be seen for $S_1 \leftarrow S_0$, (Figure 21) anti-symmetric modes like 1535 cm^{-1} can perturb the ground state anti-symmetrically, thus creating a more symmetric orbital. This perturbed orbital then enables a stronger two-photon transition to the symmetric LUMO orbital. Once excited to the symmetric LUMO, a one-photon transition is allowed down to the anti-symmetric HOMO. These theoretical studies provide an interesting physical insight into the method of Herzberg-Teller coupling in the resonance hyper-Raman spectrum. In this transition, one side of the xanthene ring in Rhodamine, acting as an electron-donating group (Figure 21, upper right – red), utilizes the pi backbone of the xanthene structure to transfer electron density to the other side of the xanthene ring, which acts as an electron-accepting group (Figure 21, upper right – green). Therefore, the nonlinear optical properties of the molecule become enhanced as indicated by the intense resonance contribution of the mode to the hyper-Raman spectrum. In this manner, R6G behaves much like a push-pull chromophore, a molecule with donating and accepting groups which has enhanced nonlinear optical characteristics.[62] Without the use of resonance hyper-Raman experiments and simulations, the push-pull character of R6G would not be identifiable.

In the $S_2 \leftarrow S_0$ transition (Figure 22), the two-photon transition from symmetric HOMO-1 to symmetric LUMO is strongly allowed. In this case, anti-symmetric

modes like 1535 cm^{-1} can induce anti-symmetry into the otherwise symmetric HOMO-1. This allows the one-photon transition from LUMO to the perturbed HOMO-1. The reason that both S_2 and S_1 appear to have the same resonant modes is that the modes show different activities in each hyper-Raman transition. In S_1, the modes are B_2 active, while in S_2, they are mostly B_1 active (though they exhibit some B_2 activity as well.) Similar to the behavior observed for $S_1 \leftarrow S_0$, R6G behaves as a push-pull chromophore in this instance, as well. The push-pull character, however, is utilized in this mode to enhance a single photon transition, instead of a two-photon transition.

Conclusion

Rhodamine 6G has served as a benchmark molecule in fields such as surface enhanced spectroscopy and two-photon imaging. Despite its widespread use, detailed assignments of the two-photon absorption spectrum have been lacking. In this study, we find that the resonance hyper-Raman scattering of R6G demonstrates both Franck-Condon (A-term) and Herzberg-Teller (B-term) coupling; and these features are further carried into the more averaged features of its absorption spectrum. In the examination of vibronic coupling, it is evident that the reason both SERS at 532 nm and SEHRS at 1064 nm spectra of Rhodamine 6G are resonant is that both experience different types of resonant scattering. Only with examining both A and B-term scattering calculations, the two-photon properties of this rich molecule can be fully understood.

CHAPTER III REFERENCES

1. He, G. S.; Tan, L. S.; Zheng, Q.; Prasad, P. N. Multiphoton absorbing materials: Molecular designs, characterizations, and applications. *Chem. Rev.* 2008, *108* (4), 1245-1330.
2. Shalav, A.; Richards, B. S.; Green, M. A. Luminescent layers for enhanced silicon solar cell performance: Up-conversion. *Solar En. Mat. and Solar Cells* 2007, *91* (9), 829-842.
3. van der Ende, B. M.; Aarts, L.; Meijerink, A. Lanthanide ions as spectral converters for solar cells. *Phys. Chem. Chem. Phys.* 2009, *11* (47), 11081-11095.
4. Hales, J. M.; Matichak, J.; Barlow, S.; Ohira, S.; Yesudas, K.; Bredas, J. L.; Perry, J. W.; Marder, S. R. Design of polymethine dyes with large third-order optical nonlinearities and loss figures of merit. *Science* 2010, *327* (5972), 1485-1488.
5. He, G. S., et al. Twisted pi-system chromophores for all-optical switching. *J. Am. Chem. Soc.* 2011, *133* (17), 6675-6680.
6. Iliopoulos, K.; Krupka, O.; Gindre, D.; Salle, M. Reversible two-photon optical data storage in coumarin-based copolymers. *J. Am. Chem. Soc.* 2010, *132* (41), 14343-14345.
7. Kawata, S.; Kawata, Y. Three-dimensional optical data storage using photochromic materials. *Chem. Rev.* 2000, *100* (5), 1777-1788.

8. Cumpston, B. H., et al. Two-photon polymerization initiators for three-dimensional optical data storage and microfabrication. *Nature* 1999, *398* (6722), 51-54.
9. Li, L. J.; Gattass, R. R.; Gershgoren, E.; Hwang, H.; Fourkas, J. T. Achieving lambda/20 resolution by one-color initiation and deactivation of polymerization. *Science* 2009, *324* (5929), 910-913.
10. Larson, D. R.; Zipfel, W. R.; Williams, R. M.; Clark, S. W.; Bruchez, M. P.; Wise, F. W.; Webb, W. W. Water-soluble quantum dots for multiphoton fluorescence imaging in vivo. *Science* 2003, *300* (5624), 1434-1436.
11. Lee, J. H.; Lim, C. S.; Tian, Y. S.; Han, J. H.; Cho, B. R. A two-photon fluorescent probe for thiols in live cells and tissues. *J. Am. Chem. Soc.* 2010, *132* (4), 1216-1218.
12. Masanta, G.; Lim, C. S.; Kim, H. J.; Han, J. H.; Kim, H. M.; Cho, B. R. A mitochondrial-targeted two-photon probe for zinc ion. *J. Am. Chem. Soc.* 2011, *133* (15), 5698-5700.
13. So, P. T. C.; Dong, C. Y.; Masters, B. R.; Berland, K. M. Two-photon excitation fluorescence microscopy. *Ann. Rev. of Biomed. Eng.* 2000, *2*, 399-429.
14. Warther, D.; Gug, S.; Specht, A.; Bolze, F.; Nicoud, J. F.; Mourot, A.; Goeldner, M. Two-photon uncaging: New prospects in neuroscience and cellular biology. *Bio. & Med. Chem.* 2010, *18* (22), 7753-7758.

15. Terhune, R. W.; Maker, P. D.; Savage, C. M. Measurements of nonlinear light scattering. *Phys. Rev. Lett.* 1965, *14* (17), 681-695.
16. Kelley, A. M., Hyper-Raman scattering by molecular vibrations. In *Annual review of physical chemistry, vol 61*, 2010; Vol. 61, 41-61.
17. Denk, W.; Strickler, J. H.; Webb, W. W. 2-photon laser scanning fluorescence microscopy. *Science* 1990, *248* (4951), 73-76.
18. Ziegler, L. D. Hyper-Raman spectroscopy. *J. Raman Spect.* 1990, *21* (12), 769-779.
19. Baranov, A. V.; Bobovich, Y. S. Super-enhanced hyper-Raman scattering from dyes adsorbed on colloidal silver particles. *Jetp Lett.* 1982, *36* (8), 339-343.
20. Baranov, A. V.; Bobovich, Y. S. Higher-order surface-enhanced Raman-scattering. *Jetp Lett.* 1982, *35* (4), 181-183.
21. Nie, S. M.; Lipscomb, L. A.; Feng, S.; Yu, N. T. Resonant and nonresonant surface-enhanced hyper-Raman spectroscopy with a picosecond laser - effect of the excitation pulse width. *Chem. Phys. Lett.* 1990, *167* (1-2), 35-40.
22. Kneipp, K.; Kneipp, H.; Seifert, F. Near-infrared excitation profile study of surface-enhanced hyper-Raman scattering and surface-enhanced Raman-scattering by means of tunable mode-locked ti-sapphire laser excitation. *Chem. Phys. Lett.* 1995, *233* (5-6), 519-524.
23. Yang, W. H.; Hulteen, J.; Schatz, G. C.; VanDuyne, R. P. A surface-enhanced hyper-Raman and surface-enhanced Raman scattering study of

trans-1,2-bis(4-pyridyl)ethylene adsorbed onto silver film over nanosphere electrodes. Vibrational assignments: Experiment and theory. *J. Chem. Phys.* 1996, *104* (11), 4313-4323.

24. Itoh, T.; Ozaki, Y.; Yoshikawa, H.; Ihama, T.; Masuhara, H. Hyper-rayleigh scattering and hyper-Raman scattering of dye-adsorbed silver nanoparticles induced by a focused continuous-wave near-infrared laser. *Appl. Phys. Lett.* 2006, *88* (8), 084102:1-10.
25. Kneipp, J.; Kneipp, H.; Kneipp, K. Two-photon vibrational spectroscopy for biosciences based on surface-enhanced hyper-Raman scattering. *Proc. Nat. Acad. Sci. USA* 2006, *103* (46), 17149-17153.
26. Leng, W.; Kelley, A. M. Hyper-rayleigh and hyper-Raman scatterings with intermediate and two-photon resonances. *J. Chem. Phys.* 2007, *127* (16), 164509: 1-23.
27. Itoh, T.; Yoshikawa, H.; Yoshida, K.; Biju, V.; Ishikawa, M. Evaluation of electromagnetic enhancement of surface enhanced hyper-Raman scattering using plasmonic properties of binary active sites in single ag nanoaggregates. *J. Chem. Phys.* 2009, *130*, 214706:1-22.
28. Itoh, T.; Yoshikawa, H.; Yoshida, K.; Biju, V.; Ishikawa, M. Spectral variations in background light emission of surface-enhanced resonance hyper-Raman scattering coupled with plasma resonance of individual silver nanoaggregates. *J. Chem. Phys.* 2010, *133* (14), 124704:1-18.

29. Long, D. A.; Stanton, L. Studies of nonlinear phenomena .1. Theory of hyper-Raman effect. *Proc. Royal Soc. Lond.* 1970, *318* (1535), 441-465.
30. Hildebrandt, P.; Stockburger, M. Surface-enhanced resonance Raman-spectroscopy of rhodamine-6g adsorbed on colloidal silver. *J. Phys. Chem.* 1984, *88* (24), 5935-5944.
31. Baranov, A. V.; Bobovich, Y. S.; Petrov, V. Spectroscopy of resonance hyper-Raman scattering of light. *Sov. Phys. Usp.* 1990, *33*, 812-832.
32. Baranov, A. V.; Bobovich, Y. S.; Petrov, V. I. Surface-enhanced resonance hyper-Raman (serhr) spectroscopy of photochromatic molecules. *J. Raman Spect.* 1993, *24*, 695-697.
33. Li, W. H.; Li, X. Y.; Yu, N. T. Surface-enhanced resonance hyper-Raman scattering and surface-enhanced resonance Raman scattering of dyes adsorbed on silver electrode and silver colloid: A comparison study. *Chem. Phys. Lett.* 1999, *312* (1), 28-36.
34. Kelley, A. M.; Leng, W. N.; Blanchard-Desce, M. Resonance hyper-Raman scattering from conjugated organic donor-acceptor "push-pull" chromophores with large first hyperpolarizabilities. *J. Am. Chem. Soc.* 2003, *125* (35), 10520-10521.
35. Kelley, A. M. Resonance Raman and resonance hyper-Raman intensities: Structure and dynamics of molecular excited states in solution. *J. Phys. Chem. A* 2008, *112* (47), 11975-11991.

36. Milojevich, C. B.; Silverstein, D. W.; Jensen, L.; Camden, J. P. Probing two-photon properties of molecules: Large non-condon effects dominate the resonance hyper-Raman scattering of rhodamine 6g. *J. Am. Chem. Soc.* 2011, *133* (37), 14590-14592.
37. Milojevich, C. B.; Silverstein, D. W.; Jensen, L.; Camden, J. P. Probing one-photon inaccessible electronic states with high sensitivity: Wavelength scanned surface enhanced hyper-Raman scattering. *ChemPhysChem* 2011, *12* (1), 101-103.
38. Wakebe, T.; Van Keuren, E. The excitation spectra of two-photon induced fluorescence in xanthene dyes. *Jpn. J. Appl. Phys. Part 1 - Regul. Pap. Short Notes Rev. Pap.* 1999, *38* (6A), 3556-3561.
39. Wolff, J. J.; Wortmann, R., Organic materials for second-order non-linear optics. In *Advances in physical organic chemistry*, Bethell, D., Ed. Academic Press: 1999; Vol. Volume 32, 121-217.
40. Yu, N. T.; Nie, S. M.; Lipscomb, L. A. Surface-enhanced hyper-Raman spectroscopy with a picosecond laser - new vibrational information for noncentrosymmetric carbocyanine molecules adsorbed on colloidal silver. *J. Raman Spect.* 1990, *21* (12), 797-802.
41. Xu, C.; Webb, W. W. Measurement of two-photon excitation cross sections of molecular fluorophores with data from 690 to 1050 nm. *J Opt. Soc. Am. B* 1996, *13* (3), 481-491.

42. Makarov, N. S.; Drobizhev, M.; Rebane, A. Two-photon absorption standards in the 550-1600 nm excitation wavelength range. *Opt. Express* 2008, *16* (6), 4029-4047.
43. Chung, Y. C.; Ziegler, L. D. The vibronic theory of resonance hyper-Raman scattering. *J. Chem. Phys.* 1988, *88* (12), 7287-7294.
44. Tannor, D. J.; Heller, E. J. Polyatomic Raman-scattering for general harmonic potentials. *J. Chem. Phys.* 1982, *77* (1), 202-218.
45. Heller, E. J.; Sundberg, R. L.; Tannor, D. Simple aspects of Raman-scattering. *J. Phys. Chem.* 1982, *86* (10), 1822-1833.
46. Heller, E. J. The semi-classical way to molecular-spectroscopy. *Accounts Chem. Res.* 1981, *14* (12), 368-375.
47. Lee, S. Y.; Heller, E. J. Time-dependent theory of Raman-scattering. *J. Chem. Phys.* 1979, *71* (12), 4777-4788.
48. Heller, E. J. Frozen gaussians - a very simple semi-classical approximation. *J. Chem. Phys.* 1981, *75* (6), 2923-2931.
49. Shoute, L. C. T.; Bartholomew, G. P.; Bazan, G. C.; Kelley, A. M. Resonance hyper-Raman excitation profiles of a donor-acceptor substituted distyrylbenzene: One-photon and two-photon states. *J. Chem. Phys.* 2005, *122* (18), 18450-18458.
50. Shoute, L. C. T.; Woo, H. Y.; Vak, D.; Bazan, G. C.; Kelley, A. M. Solvent effects on resonant first hyperpolarizabilities and Raman and hyper-Raman

spectra of dans and a water-soluble analog. *J. Chem. Phys.* 2006, *125* (5), 054506: 1-15.

51. Shoute, L. C. T.; Blanchard-Desce, M.; Kelley, A. M. Resonance hyper-Raman excitation profiles and two-photon states of a donor-acceptor substituted polyene. *J. Phys. Chem. A* 2005, *109* (46), 10503-10511.
52. Albrecht, A. C. Theory of Raman intensities. *J. Chem. Phys.* 1961, *34* (5), 1476-1485.
53. Tang, J.; Albrecht, A. C. Studies in Raman intensity theory. *J. Chem. Phys.* 1968, *49* (3), 1144-1154.
54. Albrecht, A. C.; Hutley, M. C. Dependence of vibrational Raman intensity on wavelength of incident light. *J. Chem. Phys.* 1971, *55* (9), 4438-4447.
55. Lee, P. C.; Meisel, D. Adsorption and surface-enhanced Raman of dyes on silver and gold sols. *J. Phys. Chem.* 1982, *86* (17), 3391-3395.
56. Valiev, M., et al. Nwchem: A comprehensive and scalable open-source solution for large scale molecular simulations. *Comput. Phys. Commun.* 2010, *181* (9), 1477-1489.
57. DALTON, A molecular electronic structure program, release 2.0; 2005, see http://www.kjemi.uio.no/software/dalton/dalton.html.
58. Silverstein, D. W.; Jensen, L. Vibronic coupling simulations for linear and nonlinear optical processes: Simulation results. *J. Chem. Phys.* 2012, *136* (6), 064110: 1-14.

59. Silverstein, D. W.; Jensen, L. Vibronic coupling simulations for linear and nonlinear optical processes: Theory. *J. Chem. Phys.* 2012, *136* (6), 064111: 1-13.

60. Guthmuller, J.; Champagne, B. Resonance Raman scattering of rhodamine 6g as calculated by time-dependent density functional theory: Vibronic and solvent effects. *J. Phys. Chem. A* 2008, *112* (14), 3215-3223.

61. Murugan, N. A.; Kongsted, J.; Rinkevicius, Z.; Aidas, K.; Mikkelsen, K. V.; Agren, H. Hybrid density functional theory/molecular mechanics calculations of two-photon absorption of dimethylamino nitro stilbene in solution. *Phys. Chem. Chem. Phys.* 2011, *13* (27), 12506-12516.

62. Milian, B.; Orti, E.; Hernandez, V.; Navarrete, J. T. L.; Otsubo, T. Spectroscopic and theoretical study of push-pull chromophores containing thiophene-based quinonoid structures as electron spacers. *J. Phys. Chem. B* 2003, *107* (44), 12175-12183.

CONCLUSION

Hyper-Raman spectroscopy serves as a robust method for determining the multi-photon properties of molecules. In the case of Rhodamine, coupling hyper-Raman spectroscopy with theoretical calculations allows for the probing of molecular states which are inaccessible to linear spectroscopies. Hyper-Raman scattering also yields greater vibrational coupling than expected, at least for molecules which have two-photon accessible states which are not one-photon accessible. And finally, the mechanisms in hyper-Raman scattering that lead to vibrational coupling can be used to engineer strong two-photon absorptions in a molecule. Due to these reasons, hyper-Raman spectroscopy is an important tool to use in understanding the multi-photon properties of molecules.

VITA

Christopher Bennett Milojevich was born July 20, 1981. He graduated from Wofford College in 2003 with a BS in Chemistry. After graduation, he went to Wake Forrest University to complete his Master's in Education in 2004. He spent two years teaching Chemistry at Woodruff High School in Woodruff, SC. Chris then spent two years teaching AP Chemistry at his Alma Mater, Dorman High School in Spartanburg, SC. After deciding to take on a new challenge, he came to the University of Tennessee, where he joined the Camden Group, to study Analytical Chemistry. His research concentrated on the intersection of surface spectroscopy and nonlinear spectroscopy.